Experimental investigations about complex non-relaxing fatigue loads for carbon-black filled natural rubber

I. Warneboldt, Yann Marco, P. Charrier, W. Hervouet, C. Champy, I. Raoult, V. Le Saux, F. Szmytka

Version of Record: https://www.sciencedirect.com/science/article/pii/S0142112321005375
Manuscript_cb05ddbe03bef98c57bd95346fc4c1f7

Experimental investigations about complex non-relaxing fatigue loads for carbon-black filled natural rubber

I. Warneboldt[1,2,3], Y. Marco[2], P. Charrier[1], W. Hervouet[1], C. Champy[1], I. Raoult[4], V. Le Saux[2], F. Szmytka[3]

[1]*Vibracoustic Nantes, CAE & Durability Prediction Department, 44474 Carquefou, France*
[2]*ENSTA Bretagne, UMR CNRS 6027, IRDL, 29200 Brest, France*
[3]*ENSTA Paris, IMSIA - UMR EDF/CNRS/CEA/ENSTA 9219, UME, 91120 Palaiseau, France*
[4]*Stellantis, Scientific and Future Technologies Department, 78943 Vélizy-Villacoublay, France*
email of the corresponding author: iona.warneboldt@vibracoustic.com

Abstract
This paper presents an extensive test campaign and analysis to better understand the fatigue behavior and the mechanisms at stake for natural rubber under complex non-relaxing loads. This database includes relaxing uniaxial tests under tension and torsion, relaxing and non-relaxing tension tests for 3 temperatures, relaxing multiaxial tension-torsion proportional tests, and non-relaxing tension-torsion multiaxial sequenced tests for different temperatures. The tests are conducted on hourglass-shaped natural rubber specimens, loaded by coupled and aligned tension and torsion actuators. Various strain ratios, uniaxial and biaxial loading sequences and critical plane orientation histories over a loading cycle are achieved. A total of 240 specimens were tested. Different temperatures are imposed to affect reinforcement and provide a comparison to previous results on crystallization. Furthermore, finite element analyses (FEA) are performed to determine first the respective local mechanical state in the specimens and then to infer the crack orientation predicted from a critical plane approach based on the maximum principal strain. Finally, the results are carefully analyzed based on three indicators: the relative improvement on fatigue lifetime, the cracks features (roughness and branching, from optical and SEM observations) and their comparison to the crack orientation predicted using the critical plane approach.

1. Introduction

Facing competitive and evolutive markets, the automotive industry tends to decrease dedicated times to the development phases for new products. Hence, it is a mandatory requirement to use simulation methods and consequently, to numerically design a well-engineered part before performing the prototype tests. A vehicle is however constantly exposed to random excitations from the road and periodic vibrations, *e.g.,* from its combustion engine. Therefore, the fatigue design of its components is of major importance. Furthermore, the industrial trend toward ever longer warranty periods requires more and more fatigue-design efforts to secure the demanded lifetimes. This research work thus contributes to the development of fatigue behavior predictions for anti-vibration rubber parts. Common examples are the engine and chassis mounts used to isolate the passenger compartment from the outer vibrations and excitations.

Those products undergo complex and multi-directional fatigue loads, which must be considered for their numerical design and experimental validation. Some parts must endure Road Load Data test-loads (*i.e.*, random-like, variable amplitude signals, representative of the actual service conditions of a part). Moreover, they might be additionally pre-loaded with a constant static force or displacement by the engine mass or by swaging using metallic inserts. These conditions often locally result in positive minimal load values called hereafter, non-relaxing loads. This situation is distinctive from relaxing loads, where the local mechanical variables return regularly to

zero. A mechanical cycle is therefore defined as *relaxing*, if the sample is unloaded at some time during the cycle. On a local scale, it means that the temporal evolution of a given parameter (*e.g.*, the strain) crosses zero. Otherwise, the mechanical cycle is referred to as *non-relaxing*. A short discussion is here useful on the definition of relaxing and non-relaxing terms. In this paper, the definition of the relaxing or non-relaxing nature of a given test condition is based on the R-ratio computed from displacements or angles. It is a global definition, often met in the literature [1–3]. Nevertheless, a definition based on local tensors is disputable, even more in the case of multi-axial tests. This is the reason why here non-relaxing or relaxing terms should be seen as *a priori* tests classification. The real evaluation of the nature of the test conditions is based on the observed (or not) reinforcement on fatigue lifetime. For natural rubber (NR), non-relaxing conditions lead to local material reinforcement, which results in an increase of the fatigue lifetime. In some applications, *e.g.*, when parts are highly swaged, this effect is used to design more durable parts. As early as 1940, Cadwell *et al.* [4] demonstrated a reinforcement effect of NR specimens when submitted to non-relaxing tension loads. They studied different cylindrical rubber specimens under constant displacement amplitudes, varying the minimum displacement levels from one test to another. Compared to tests performed under relaxing loading conditions, the results highlighted a lifetime increase of up to more than a factor of 100 for some non-relaxing displacement levels. A clear way to illustrate the reinforcement effect on specimen lifetimes is to plot the Haigh diagram. An example of such a diagram for natural rubber is given in *Figure 1*.

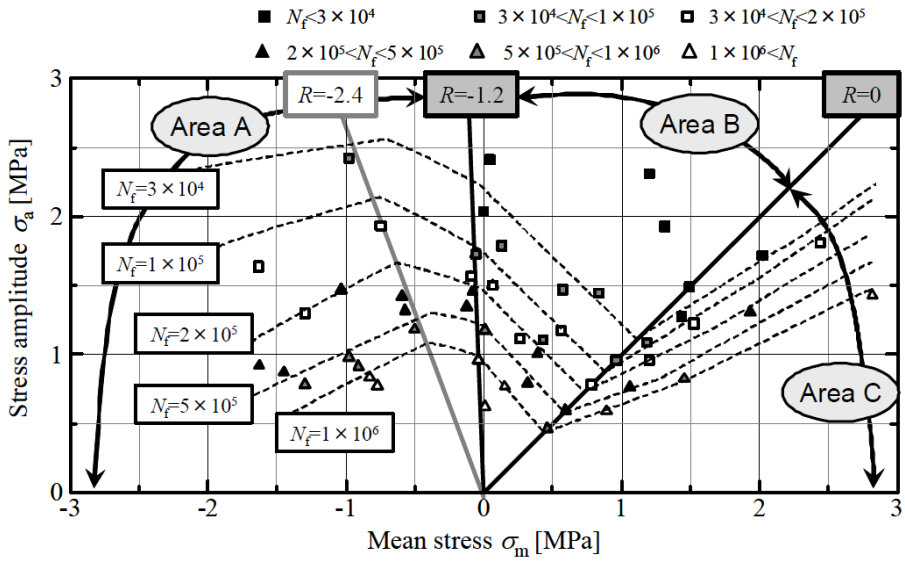

Figure 1: Wide-range Haigh diagram from Oshima *et al.* [5].

It exhibits on the ordinate as indicator of the load amplitude (here the stress) and on the abscissa the mean load value. The plotted lines represent loading conditions for iso-lifetime. The "Area C" of the given Haigh diagram is of primary interest as it demonstrates the reinforcement effect since a higher mean stress level results in a higher lifetime for the same stress amplitude. At this stage, it is crucial to underline that the application of the Haigh

diagram is almost always limited to uniaxial signals. However, to be able to determine a mean-load correction factor for a part or a specimen under complex variable amplitude loads, the definition of non-relaxing loading and the concept of the Haigh diagram must be extended to multiaxial situations. Nevertheless, few studies investigate the reinforcement effect of NR under multiaxial solicitations [6,7]. This question is within the scope of this paper.

To explain this local reinforcement effect (*i.e.*, longer lifetime under higher mean load and equal load amplitude), it is possible to invoke the substantial modifications of the crack surface roughness, patterns and cyclic propagation rate. Some careful investigations on the crack orientations and patterns are given in the literature, to better understand the link between crack evolution and the initiation criteria. The following summarizes those findings regarding non-relaxing fatigue loads for natural rubber. Busse published first studies in 1935 [8] on "rectangular tear samples". He reports observations for high minimal tension loads, when propagating pre-cut cracks under tension-tension loads. With a global minimal stretch of 15%, or higher, he observes that the main crack propagation path would split in two separate paths shortly after starting the cyclic loads. The two separate crack tips propagate in an almost vertical direction, parallel to the load, or even backwards with higher minimal stretch (see *Figure 2*).

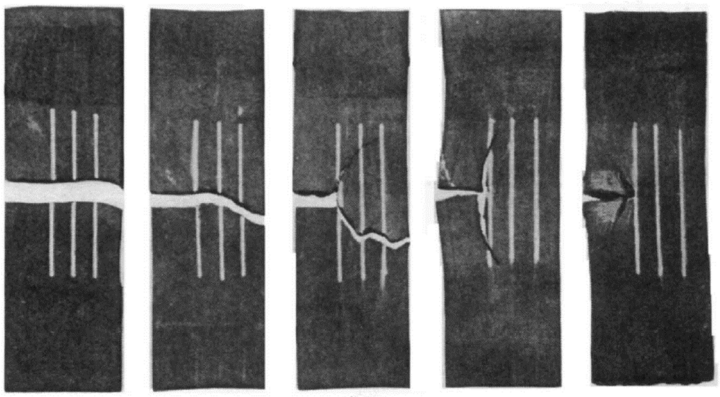

Figure 2: Findings of Busse in [8] for tests with a maximal nominal stretch of 160%. The minimal stretches are from left to right: 105%, 110%, 115%, 117%, 120%.

In a more recent study, Champy *et al.* [9] characterize the fatigue damage mechanisms, observed for (highly-) non-relaxing tension loads on hourglass-shaped AE2 specimens of natural rubber. They describe appearance of peels with shapes depending on the tension load ratio (see *Figure 3*). The authors report that cracks start growing perpendicular to the loading directions. Then, at some point of the fatigue test, a sudden and quick deviation of the propagation along the load-parallel direction occurs, which explains the observed peels.

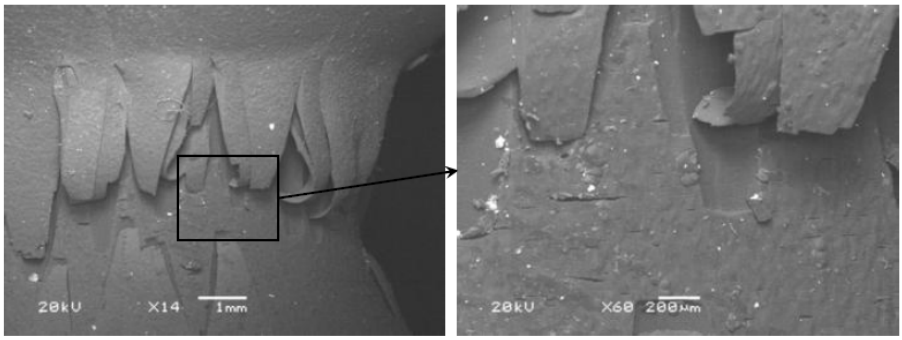

Figure 3: Observed peels for non-relaxing tests with a displacement R-ratio (min. displacement/max. displacement) of 0.82; from [9].

Saintier *et al*. also described this bifurcation effect [10] when studying the shape of small macro-cracks of diabolo-shaped natural rubber specimens under relaxing and non-relaxing tension-loadings. They report that the cracks appear in both cases in the orthogonal plane of the loading direction. However, they describe "crack-branching" (splitting of a crack in two or more cracks) for the non-relaxing tests. *Figure 4* gives SEM images of both test conditions, relaxing and non-relaxing. It is also interesting to underline on these SEM pictures that the early stages of the crack branching effect led to a more visible roughness of the fatigue cracks under non-relaxing loading.

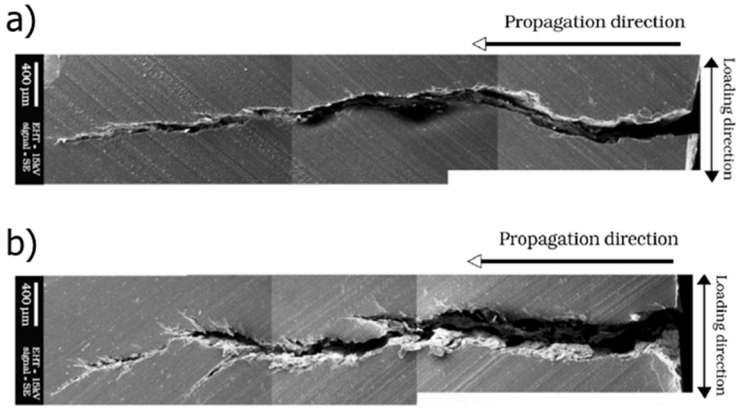

Figure 4: Crack shape observations of Saintier *et al*. for a) relaxing and b) non-relaxing tension tests (from [10]).

These three studies illustrate that non-relaxing conditions lead to specific crack features: crack bifurcation and higher crack roughness. These two microscopic features come with a reduced crack growth rate, as illustrated in *Figure 5* and demonstrated by many studies [11–13].

Moreover, the crack propagation orientation is of primary interest to describe the fatigue resistance of materials, especially to understand the links between microstructure, loading conditions and lifetime. The usual observation is that the crack orientation is perpendicular to the highest maximal principal stress or respectively stretch[1] (often

[1] For isotropic models (like commonly used for rubbers), the directions of the highest maximal principal stress and strain are the same.

referenced as the critical plane), at least for load ratios of R=0 (*i.e.*, relaxing loads). This observation seems verified also for cyclic multiaxial loads (see for instance [6,14,15]).

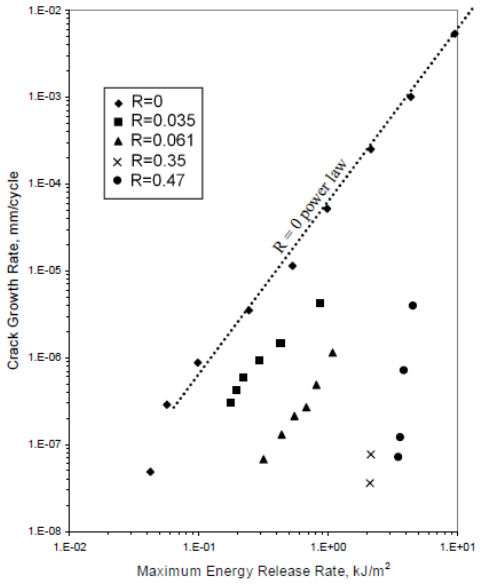

Figure 5: Crack growth rate of NR samples with different load ratios, from [16], with test results of [17]. The load ratios are given as the ratio between maximal and minimal tear energy after Griffith [18].

The experimental observations of crack branching [8–10] illustrates that the crack propagation plane is not anymore in accordance with the critical plane for non-relaxing conditions, but no studies thoroughly checked this fact under multiaxial loads. Hence, in this paper, a systematic comparison between crack orientations determined for all conducted fatigue tests and computed critical planes is performed.

The reinforcement effect and modifications of the cracks features and propagation rate for NR are very often related to the strain induced crystallization (SIC), which was first reported for this material by Katz in 1925 [19] while an extensive review of SIC in natural rubber is given by Huneau [20]. A way to illustrate the importance of crystallization on the fatigue properties of NR is to compare the fatigue properties of crystallizing and non-crystallizing compounds (see [21] for example on crack propagation). Another way is to investigate the crystallinity ratio on rubber samples or at the crack tip under cyclic loading (see for instance, [22–24]). In particular, Beurrot-Borgarino *et al.* [25] show that a positive load ratio has a strong influence on the amount of crystallinity during fatigue tests (see *Figure 6*). These careful studies illustrate that crystallization is a key factor (even if not the only one, probably) for the understanding of the improvement of the fatigue lifetime under non-relaxing conditions.

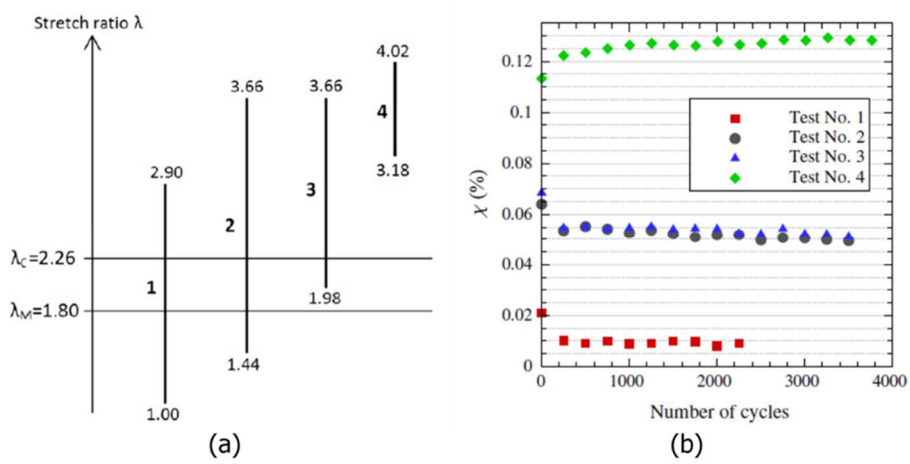

Figure 6: Strain-induced crystallization of carbon black-filled natural rubber during fatigue measured by in situ synchrotron X-ray diffraction: (a) Four different stretch ratios tested, with given minimal and maximal stretch level; (b) Evolution of the crystallinity index during fatigue tests; from [25].

Nevertheless, Wide Angle X-ray Diffraction is the only way to have direct access to the crystallinity. The literature illustrates how complex this investigation might be when it comes to investigations on massive samples, and even more under multiaxial fatigue loading [23]. Another interesting way to illustrate the effect of crystallization on fatigue resistance is to perform tests at different temperatures. Indeed, temperature has a major influence on the fatigue behavior of natural rubber. Early studies by Cadwell *et al.* [4] report decreasing lifetimes with increasing material temperatures, more recent studies of temperature influence are given by Charrier *et al.* [26]. Even if this effect might not be related only to strain-induced crystallization, it seems to be a major factor. Marchal [27] specified that a higher temperature reduces the maximal density of crystallites for natural rubber and that higher local stretches are required to detect crystallization. The author states that no crystallites were found with a test temperature of 82°C and higher. These observations stem a convenient way to illustrate the influence of SIC on fatigue lifetime and we will therefore consider it in this study.

Figure 7 wraps up the different observations from the literature relevant to this paper. The overall industrial goal is to relate crack features and the lifetime reinforcement in order to improve understanding of the related fatigue phenomena. To do so, it is first mandatory to have access to a large database giving not only the conditions required to observe reinforcement but also to quantify this effect. Even under uniaxial loading, these results remain rare in the published literature [4,5,9]. This conclusion is even truer for multiaxial loading [7]. To our knowledge, no reference work providing an extensive and quantitative database is available yet. Therefore, the first objective of this study is to provide a quantitative database on lifetime reinforcement under tension-torsion loading, both for relaxing and non-relaxing conditions.

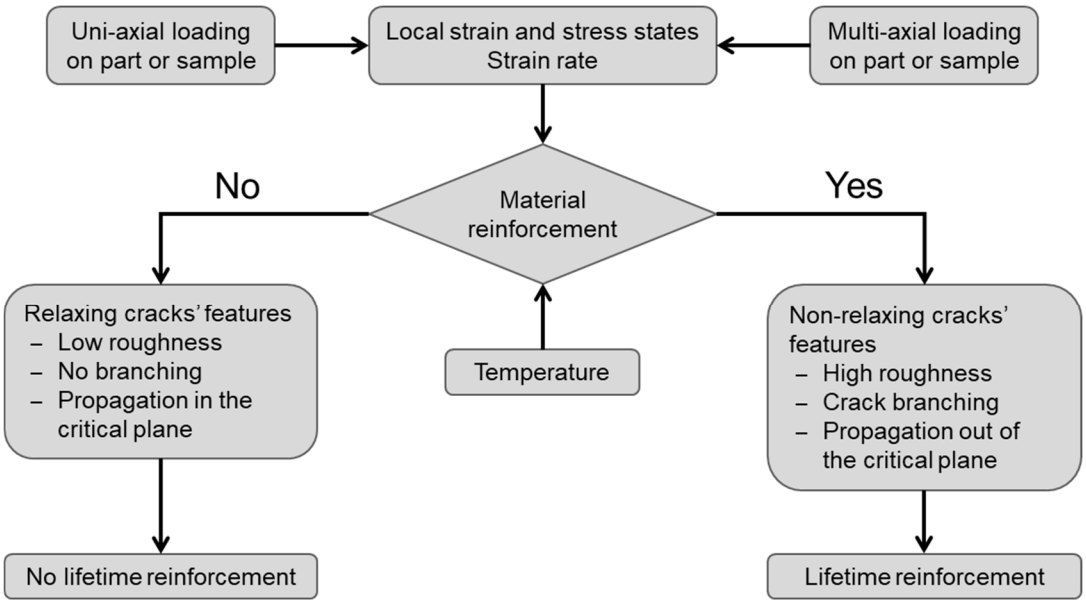

Figure 7: Different observations concerning material reinforcement described in the literature.

Another important aspect for parts design is to determine the locations and directions of fatigue cracks. To do so, a common way is to compute a fatigue indicator value from the local mechanical field, combined to a critical plane approach. This approach seems to give reasonable results under uniaxial and multiaxial relaxing loads, as cracks propagate according to the so-called critical plane [6,11,15]. Nevertheless, experimental observations illustrate that this seems not to be the case anymore for non-relaxing conditions. This observation is likely dependent on load ratio and multiaxial loading mode. Consequently, the second objective of this study is to investigate possible evolution of the deviation of crack propagation compared to the critical plane prediction under uniaxial and multiaxial conditions, for both relaxing and non-relaxing conditions.

The third objective of the study is to improve the understanding of the mechanisms at stake behind the material reinforcement. In literature, this material reinforcement is mostly related to crystallization. As no direct measurements are undertaken in this study, no direct connection will be possible. Nevertheless, the experimental database includes a large number of tests performed at various temperatures between 23 and 80°C. Taking into account that crystallization could be inhibited by high temperature, this wide database could give some hints on the connection between microscopic features (*i.e.*, cracks roughness, branching and orientation), macroscopic effects (global reinforcement) and the material crystallization and reinforcement.

This paper therefore presents an extensive test campaign and analysis to better understand the fatigue behavior and the mechanisms at stake for natural rubber under complex non-relaxing loads. This database includes relaxing uniaxial tests under tension and torsion; relaxing and non-relaxing conditions tension tests for 3 temperatures,

relaxing multiaxial tension-torsion proportional tests, and non-relaxing tension-torsion multiaxial sequenced tests for different temperatures. Section 2 provides all necessary information about the experimental set-up, specimens, and all conducted post-mortem analyses. Section 3 gives a short outline of the numerical simulations carried out to determine the critical plane directions. Section 4 gives all determined test results, enriched by the numerical results, and discusses the observations according to the questions raised in the introduction. The last section summarizes all findings and derives general conclusions.

2) Material and experimental methods

2.1. Experimental set-up

The studied material is an industrial carbon black filled natural rubber. The specimens were all manufactured under identical molding process settings and from a single material batch to ensure equal mixing and curing conditions. Different protocols are proposed to analyze its fatigue resistance.

Sample & test rig

All tests are performed with the AE2 specimen. Its geometry is detailed in *Figure 8*. The advantage of the axisymmetric, notched rubber body is its well-defined and limited zone of fatigue crack initiations in the notch area [28]. The low test-volume also reduces the heat build-up during fatigue tests.

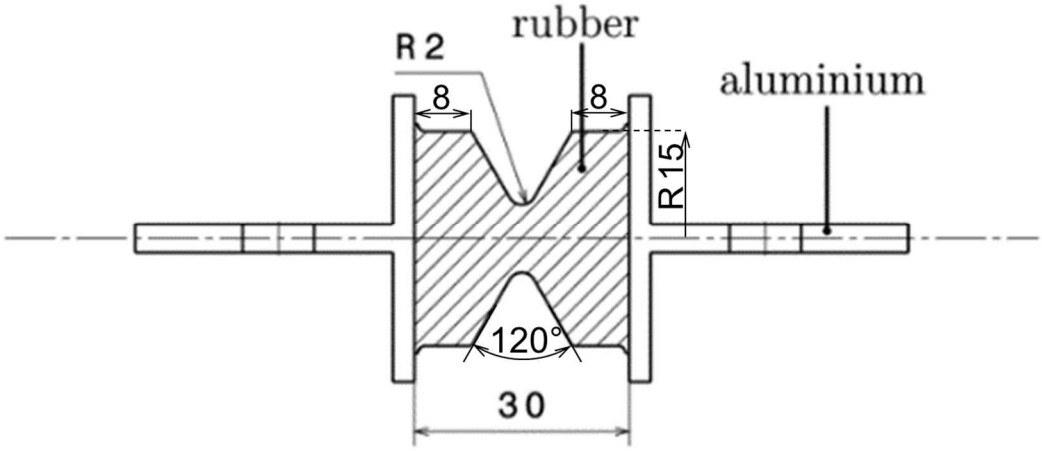

Figure 8: Geometry of the AE2 specimen, all dimensions are given in mm.

The experimental test rig is shown in *Figure 9*. Its electrical rotation and pneumatic displacement actuators are aligned and coupled. The tests are performed in a displacement/rotation-controlled manner, while the reaction force and torque are constantly recorded. The test set-up allows to track these experimental results for each

imposed cycle. A climatic chamber, enclosing the tested sample, allows to regulate the testing temperature fixed between 23°C and 80°C. This temperature is well regulated by a measurement-based control loop. An infrared sensor pointing at the notch of the specimen is measuring its surface temperature with a resolution better than ± 0.1°C.

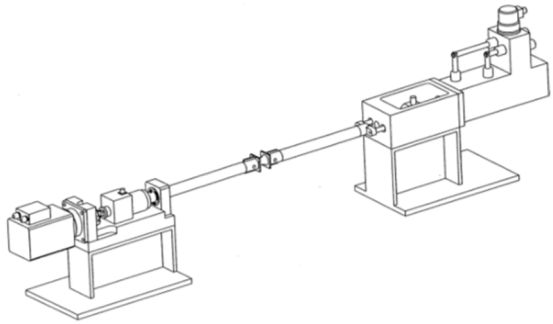

Figure 9: Test rig of coupled rotation and displacement actuators (total length: approx. 1.5m). The climate chamber is not shown.

End of life (lifetime) definition

The number of cycles to end of life N_i is determined by the $N.dk/dN$ criterion, introduced in [28]. The global stiffness of the tested specimen is indeed monitored and compared to the expected viscoelastic material behavior:

$$N\,{\mathrm{d}k}/{\mathrm{d}N} = c \tag{1}$$

where N is the number of fatigue cycles, k is the global specimen secant stiffness and c is a constant parameter. A fixed stiffness cyclic rate deviation from this law is taken as the threshold to indicate the initiation of macro-cracks of approximately 1mm length. This criterion applies to displacement stiffness and to the rotation one. For all following tests, when both actuators are in use, the rotation stiffness is used to determine N_i as it is mostly the only moving axis (pretension is applied in the tensile direction). Typical evolutions of the end-of-life criterion and of the respective stiffness amplitude history are given in *Figure 10*.

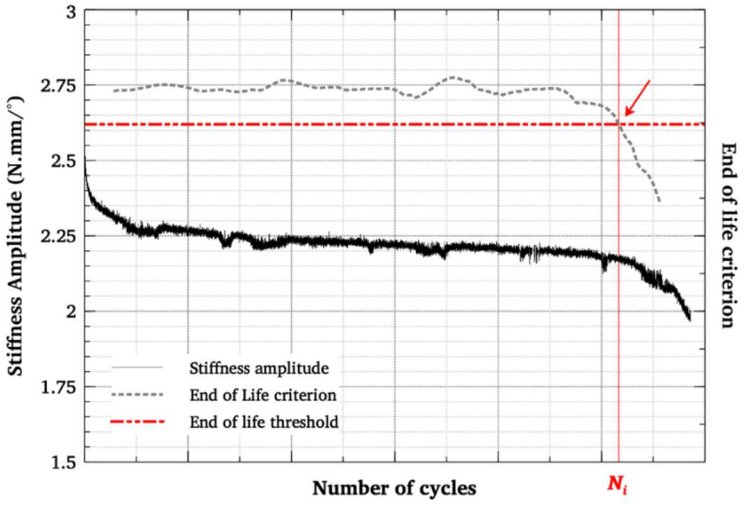

Figure 10: N dk/dN end of life criterion evolution and torsional stiffness amplitude.

Breaking pattern analysis procedure

To link the damage process to loading conditions, the fatigue crack plane orientations are of interest. A scanning electron microscope (SEM, Nikon JCM-6000) is used to analyze the surfaces of the tested samples. The metallic inserts are clamped to a dedicated mount to assure a well-controlled alignment while a "crack-opening" tilt of maximum 2° is applied to ease the detection of small cracks without significantly changing the crack orientation. Each sample is analyzed over four different points of view (each of one corresponds to a 90° rotation of the sample along its axis). Cracks smaller than 0.5mm are not considered in this study because they do not necessary exhibit a clear propagation orientation yet. The crack orientation angles are determined for all cracks appearing in the small area which could be considered almost orthogonal to the viewpoint. The considered zone is approximately 4mm wide and 4mm high, which means that around 55% of the notch ground's surface is investigated for the crack orientation analyses. An accurate angle determination outside this region is not reliable because cracks appear biased on the images due to both the lens perspective and the cylindrical shape of the sample. The derived orientation angles are defined regarding a horizontal line (in the sense of the radial axis of the specimen), as presented in *Figure 11*.

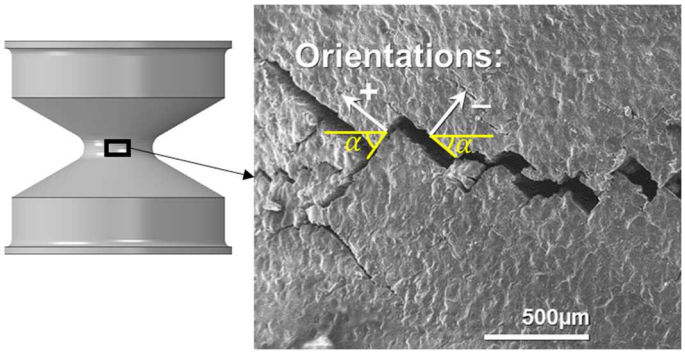

Figure 11: Breaking patterns on the surface of a tested AE2 specimen and definitions. Angles in relation to the radial plane (here the horizontal one).

Nano-indentation test protocol to avoid aging effects

The fatigue behavior of the tested rubber is known to be sensitive to material aging, especially when tested under elevated temperatures [29]. To exclude such effects from consideration for this article's study, nano-indentation tests were conducted. A specimen tested under approximately 120 000 fatigue cycles for 24h at 80°C is studied in comparison to a virgin specimen with an indentation test protocol similar to the one used by Le Gac *et al.* [30]. The used device is a Hysitron TI 980 nanoindentation platform. The specimen is cut in the radial direction close to the notch center, glued to a glass sheet and maintained using vacuum. Indentation tests are afterwards performed at the specimen's axial center and close to the skin. The results are given in *Figure 12*. Each region is tested at 5 close locations. The points represent the estimated mean value, while the error bars reflect the derived 2σ-range.

The fact that the measurements of both regions are quasi-identical for the tested and the virgin specimen leads to the conclusion that no aging effect is observable. This is due to the relatively low self-heating and to the short exposition time at elevated temperatures for the fatigue tests. Since this specimen tested at 80°C represents the most severe load level, in terms of possible aging, this effect can be excluded for all tested specimens in this article.

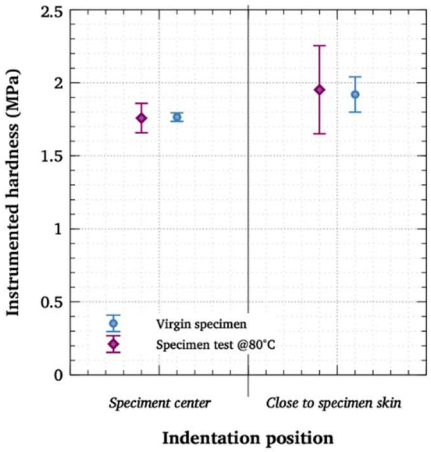

Figure 12: Results of indentation tests on specimen's cut surface.

2.2. Experimental database

As mentioned earlier, the proposed experimental base covers both tensile and torsional loading. The frequency of the cyclic load is adapted to prevent too high heat build-up. Applied frequencies of this study are between 0.8Hz to 5Hz. The target is a stationary temperature increase of maximal 10°C, measured at the outer surface of the specimen, compared to the chamber temperature. Table 1 and Table 2 give the conditions of all conducted tests. Five specimens are tested at each load level. The tables also contain test results as the reinforcement factor with reference to some given load level, statistical values of the crack orientation measurements and the comparison of calculated and measured crack orientation. For more introduction and discussion of these values, please see the following sections. The given load ratios R are defined as:

$$R_{displ} = \frac{d_{min}}{d_{max}} \tag{2}$$

$$R_{\theta} = \frac{\theta_{min}}{\theta_{max}} \tag{3}$$

$$R_{\varepsilon_1} = \frac{\varepsilon_{1min}}{\varepsilon_{1max}} = \frac{\lambda_{1min} - 1}{\lambda_{1max} - 1} \tag{4}$$

where d_{min} and d_{max} are the minimum and maximum specimen displacements; θ_{min} and θ_{max} are the minimum and maximum specimen rotation angles. ε_1 is the FEA-calculated maximal principal nominal strain which is defined as the maximal principal stretch λ_1 minus 1 (see section 3).

Table 1: Testing conditions for pure tension tests of AE2 specimen. 5 specimens were used for each condition, therefore 135 specimens in total.

Reference	Chamber temperature (°C)	Min. displacement (mm)	Max. displ. (mm)	R_{displ} (-)	R_F (-)	Fixed displ. (mm)	Min. rotation (°)	Max. rotation (°)	R_{angle} (-)	Fixed rotation (°)	Test frequency (Hz)	R_{ε_1} (-)	Measured mean reinforcement factor (-) / Reinforcement reference		Mean crack orientation (°)	Nbr of cracks measured (-)	2σ value (°)	Calculated crack orientation within 2σ-range of measurement?	Comments on cracks patterns	Illustrative figure
Wöhler_23degC	23	0	4.1	0	-0.2	-	-	-	-	0	5.0	0	-	-	Crack orientations are not measured. Observations under the optical microscope show always cracks in the expected plane perpendicular to the loading direction.	-	-	-	For reinforcement tests, effects of "crack branching" can be observed. But general propagation direction of the cracks is always the plane perpendicular to the tension load.	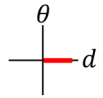
		0	5.7	0	-0.13	-	-	-	-	0	4.0	0	-	-		-	-	-		
		0	8.1	0	-0.19	-	-	-	-	0	2.5	0	1.0	Ref_W8.1mm		-	-	-		
		0	10.6	0	-0.12	-	-	-	-	0	1.5	0	1.0	Ref_W23degC		-	-	-		
Wöhler_50degC	50	0	4.1	0	-0.11	-	-	-	-	0	5.0	0	-	-		-	-	-		
		0	5.7	0	-	-	-	-	-	0	4.0	0	-	-		-	-	-		
		0	8.1	0	-	-	-	-	-	0	2.5	0	0.88	Ref_W8.1mm		-	-	-		
		0	10.6	0	-	-	-	-	-	0	1.5	0	1.0	Ref_W50degC		-	-	-		
Wöhler_80degC	80	0	4.1	0	-0.08	-	-	-	-	0	5.0	0	-	-		-	-	-		
		0	5.7	0	-	-	-	-	-	0	4.0	0	-	-		-	-	-		
		0	8.1	0	-	-	-	-	-	0	2.5	0	0.63	Ref_W8.1mm		-	-	-		
		0	10.6	0	-	-	-	-	-	0	1.5	0	1.0	Ref_W80degC		-	-	-		
Reinf_23degC	23	1.1	10.6	0.1	0.03	-	-	-	-	0	1.9	0.09	1.1			-	-	-		
		1.6	10.6	0.15	0.10	-	-	-	-	0	2.1	0.13	1.4			-	-	-		
		2.1	10.6	0.2	0.16	-	-	-	-	0	2.3	0.17	3.5	Ref_W23degC		-	-	-		
		2.65	10.6	0.25	0.18	-	-	-	-	0	2.6	0.23	18.1			-	-	-		
		3.2	10.6	0.3	0.22	-	-	-	-	0	3.0	0.28	66.8			-	-	-		
Reinf_50degC	50	1.1	10.6	0.1	0.04	-	-	-	-	0	1.9	0.09	1.2			-	-	-		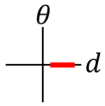
		1.6	10.6	0.15	0.11	-	-	-	-	0	2.1	0.13	1.3			-	-	-		
		2.1	10.6	0.2	0.16	-	-	-	-	0	2.3	0.17	3.1	Ref_W50degC		-	-	-		
		2.65	10.6	0.25	0.22	-	-	-	-	0	2.6	0.23	9.8			-	-	-		
		3.2	10.6	0.3	0.26	-	-	-	-	0	3.0	0.28	31.7			-	-	-		
Reinf_80degC	80	1.1	10.6	0.1	0.07	-	-	-	-	0	1.9	0.09	1.1			-	-	-		
		1.6	10.6	0.15	0.13	-	-	-	-	0	2.1	0.13	1.4			-	-	-		
		2.1	10.6	0.2	0.18	-	-	-	-	0	2.3	0.17	2.3	Ref_W80degC		-	-	-		
		2.65	10.6	0.25	0.23	-	-	-	-	0	2.6	0.23	4.0			-	-	-		
		3.2	10.6	0.3	0.27	-	-	-	-	0	3.0	0.28	11.9			-	-	-		

Table 2: Testing conditions for coupled rotation and displacement actuator setting. 5 specimens were used for each condition, therefore 105 specimens in total (np = not published).

	Reference	Chamber temperature (°C)	Min. displacement (mm)	Max. displ. (mm)	R_{displ} (-)	R_F (-)	Fixed displ. (mm)	Min. rotation (°)	Max. rotation (°)	R_{angle} (-)	R_{torque} (-)	Fixed rotation (°)	Test frequency (Hz)	R_{ε_1} (-)	Measured mean reinforcement factor (-) / Reinforcement reference		Mean crack orientation (°)	Nbr of cracks measured (-)	2σ value (°)	Calculated crack orientation within 2σ-range of measurement?	Illustrative figure
A	Pure_rot	23	-	-	-	-	0	0	150	0	-0.09	-	2.0	0	1.0	Ref_pure_rot	-28	21	19.5	Yes	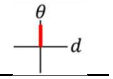
			-	-	-	-	0	-150	150	-1	-1.01	-	0.8	0	0.4 1.0	Ref_pure_rot Ref_Alt_0mm	-14.4 / 12.5	7 / 4	8.1/11.0	Yes	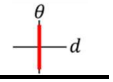
B	Sequenced_0toMax	23	-	-	-	0.53	2.5	0	150	0	-0.13	-	2	0.18	10.1 8.7	Ref_pure_rot Ref_proportional_2.5mm	-50.8	42	15.9	No	
			-	-	-	0.81	5	0	150	0	-0.16	-	1.9	0.38	42.8 1.0 46	Ref_pure_rot Ref_0tomax_5mm Ref_proportional_5mm	-62.2	43	7.1	No	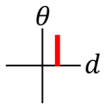
	Sequenced_50degC_0toMax	50	-	-	-	0.78	5	0	150	0	-0.07	-	1.9	0.38	0.62	Ref_0tomax_5mm	-57.0	5	2.5	No	
	Sequenced_60degC_0toMax	60	-	-	-	0.73	5	0	150	0	-0.13	-	1.9	0.38	0.37	Ref_0tomax_5mm	-52.1	15	5.8	No	
	Sequenced_70degC_0toMax	70	-	-	-	0.72	5	0	150	0	-0.12	-	1.9	0.38	0.26	Ref_0tomax_5mm	-46.9	11	6.9	No	
	Sequenced_80degC_0toMax	80	-	-	-	0.73	5	0	150	0	0.06	-	1.9	0.38	0.10 1.0	Ref_0tomax_5mm Ref_0tomax_5mm80degC	-21.2	26	23.0	Yes	
C	Sequenced_MintoMax	23	-	-	-	0.79	5	-50	150	-0.33	-0.27	-	1.5	0.38	np	-	-57.5	40	5.4	No	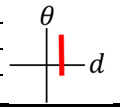
			-	-	-	0.81	5	-125	150	-0.83	-0.85	-	1.5	0.38	np	-	-58.3	48	5.5	No	
	Sequenced_80degC_mintoMax	80	-	-	-	0.70	5	-50	150	-0.33	-0.41	-	1.5	0.38	np	-	-16.5	39	14.1	Yes	
			-	-	-	0.71	5	-125	150	-0.83	-0.74	-	1.5	0.38	np	-	-13.9	27	13.8	Yes	
D	Sequenced_Alt	23	-	-	-	0.32	2.5	-150	150	-1	-1.04	-	0.8	0.18	1.42 3.5	Ref_0tomax_0mm Ref_Alt_0mm	44.2 / -45.0	25 / 24	9.2/7.0	No	
			-	-	-	0.8	5	-150	150	-1	-1.04	-	0.8	0.38	0.10 11.6	Ref_0tomax_5mm Ref_Alt_0mm	64.1 / -61.8	34 / 41	5.5/8.7	No	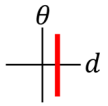
	Sequenced_50degC_Alt	50	-	-	-	0.74	5	-150	150	-1	-0.95	-	0.9	0.38	0.09	Ref_0tomax_5mm	-56.2 / 55.9	19 / 20	7.4/4.3	No	
	Sequenced_60degC_Alt	60	-	-	-	0.74	5	-150	150	-1	-0.96	-	0.9	0.38	0.07	Ref_0tomax_5mm	-45.8 / 51.1	11 / 24	28.5/22.7	No	
	Sequenced_70degC_Alt	70	-	-	-	0.72	5	-150	150	-1	-0.98	-	0.9	0.38	0.04	Ref_0tomax_5mm	-25.5 / 25.7	4 / 7	36.9/34.7	Yes	
	Sequenced_80degC_Alt	80	-	-	-	0.7	5	-150	150	-1	-1.02	-	0.9	0.38	0.01 0.14	Ref_0tomax_5mm Ref_0tomax_5mm80degC	-19.3 / 10.7	3 / 3	2.3/7.0	Yes / No (but close)	
E	Proportional_23degC	23	0	2.5	0	-0.5	-	0	150	0	-0.12	-	2	0	1.16 1	Ref_0tomax_0mm Ref_proportional_2.5mm	-27.1	38	10.0	No (but close)	
			0	5.0	0	-0.23	-	0	150	0	-0.14	-	2	0	0.93 0.02 1.0	Ref_0tomax_0mm Ref_0tomax_5mm Ref_proportional_5mm	-17.7	32	8.3	Yes	
	Proportional_80degC	80	0	5.0	0	-0.26	-	0	150	0	0.1	-	2	0	0.26 0.006 0.28	Ref_0tomax_0mm Ref_0tomax_5mm Ref_proportional_5mm	-14.5	15	13.2	Yes	

Visco-elastic effects can however lead to permanent strain and cyclic accommodation that could change the local R-ratio on strain and stress. *Figure 13* exhibits the evolution of the maximal and minimal forces during the tension tests for different R_{displ} ratios. This evolution shows that the influence of the permanent strain remains limited to low R_{displ} ratios. Nevertheless, in order to be rigorous and to provide a better description of the fatigue tests, the evolution of the force/torque load ratio is computed from the experimental results, for the full test campaign and available on Table 1 and 2 as references. As previously, these two ratios are computed as:

$$R_F = \frac{\mathcal{F}_{min}}{\mathcal{F}_{max}} \tag{5}$$

$$R_{torque} = \frac{\mathcal{T}_{min}}{\mathcal{T}_{max}} \tag{6}$$

with $\mathcal{F}_{max}$ and $\mathcal{F}_{min}$ / $\mathcal{T}_{max}$ and $\mathcal{T}_{min}$ are the mean values of the maximal and minimal measured reaction forces / torques at $N_i/2$ cycles where they can be seen as quasi-stable because the specimen global stiffness evolution during test shows an exponential decrease.

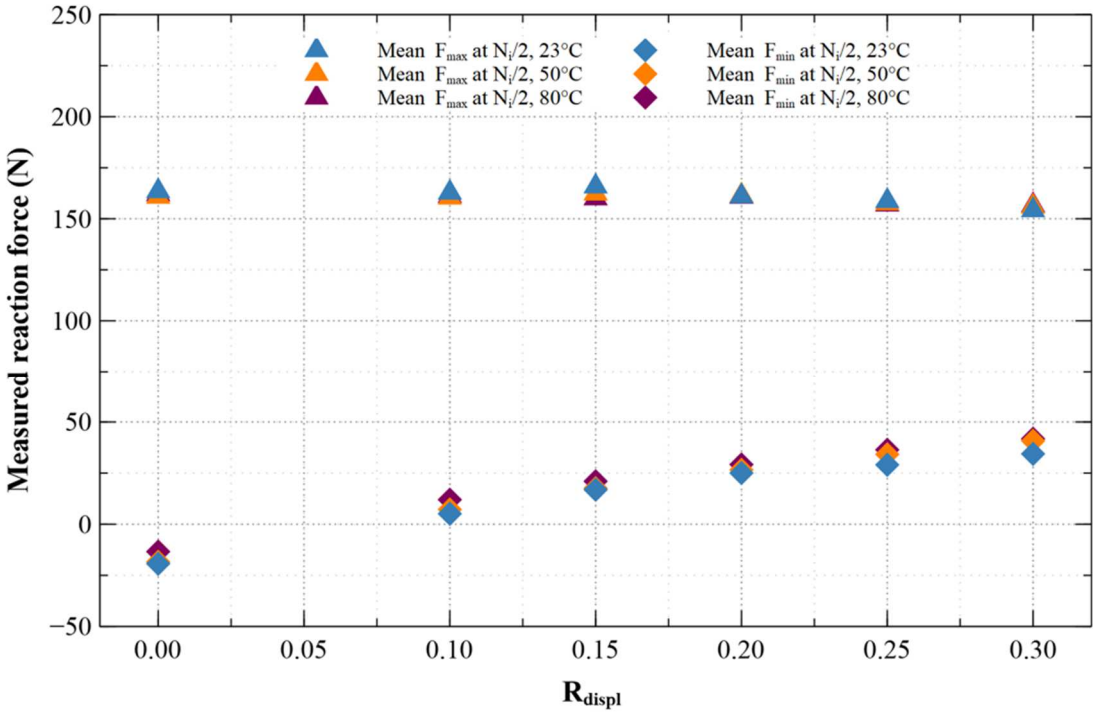

Figure 13: Mean values of measured maximal and minimal reaction forces of simple reinforcement tests at different temperatures

Relaxing material characterizations

To characterize standard fatigue properties of the material samples, tension tests are carried out to derive classical Wöhler curves. Displacement-relaxing tests are conducted with four different maximum displacement levels.

Tests are performed at three different temperatures (23, 50 and 80°C) to investigate the temperature effect for relaxing loads. Testing conditions were chosen to result in lifetimes from 5,000 to 1,000,000 cycles. The Wöhler curves are fitted with the classic Basquin's law [31]:

$$Ni = intercept \cdot (Max.displacement)^{slope} \quad (7)$$

where $intercept$ and $slope$ are Wöhler curve defining parameters.

Reinforced material characterization in pure tension

Three tension reinforcement curves are obtained to study the non-relaxing properties of the tested material (reference: Reinf_23degC, Reinf_50degC, Reinf_80degC). For each curve, the maximum displacement is kept constant at 10.6mm, while different minimum displacement levels are set. The reinforcement condition is commonly quantified with the R-ratio. Like previously for the standard Wöhler curves, three test temperatures are considered to highlight their influence on the material reinforcement (23, 50, 80°C). The reference maximum displacement is 10.6mm which, in relaxing conditions, results in lifetimes in the range of 5,000 to 20,000 cycles. Variations for the R_{displ}-values are obtained by setting different minimum. displacement conditions that are chosen to result in lifetimes that do not exceed 2,000,000 cycles to limit test duration.

Pure rotation loads

Two different kind of pure rotation tests are conducted and studied. For $R_\theta = 0$, the specimen is cyclically rotated from 0° to different maximum rotation levels. For $R_\theta = -1$, alternating rotation cycles go from a negative to a positive rotation with the same amplitude in absolute value. All tests are carried out at 23°C chamber temperature.

Proportional reference loads

Additional proportional tests are conducted. These loads are designed to impose the same maximal displacement and rotation loads as for the respective sequenced loadings that are introduced in the following. But here the minimal load levels are set to 0mm/0° to assure relaxing load conditions.

Sequenced non-relaxing loads

Some of the presented tests are already published in a conference proceeding in 2019 [32]. Coupled non-relaxing tests are based on the same set-up with a constant tensile displacement coupled with different rotation cycles and thus four different angle ratios R_θ between -1 and 0. For each load level, four to five specimens are tested. Standard test temperature is 23°C, but four elevated testing temperatures (50°C, 60°C, 70°C, 80°C) are also

investigated to highlight the influence of temperature on fatigue resistance and behavior for these specific loading conditions.

3) Theory/Calculations

3.1. FEA calculation

Finite Element Analysis (FEA) calculations are performed to evaluate local mechanical evolution in the specimen during the applied fatigue cycles. The nominal specimen geometry (see Fig. 1) is used to produce the CAE model while the software Abaqus is used with implicit calculations in geometrical nonlinear configuration.

3.1.1. Constitutive material model

The hyperelastic, isotropic, compressible Mooney-Rivlin material model is used [33,34]. The constitutive law uses the following strain energy function [35]:

$$W = C_{10}(\bar{I}_1 - 3) + C_{01}(\bar{I}_2 - 3) + \frac{1}{D_1}(J-1)^2 \qquad (8)$$

where C_{10}, C_{01}, D_1 are the material parameters, $\bar{I}_1, \bar{I}_2$ are the first and second isochoric invariants of the left Cauchy-Green deformation tensor $\boldsymbol{b} = \boldsymbol{F}\boldsymbol{F}^T$, $\boldsymbol{F}$ is the deformation gradient tensor and J is the volume change.

Because of limited temperature dependency, the parameters are regarded as constant over temperature. This can be also justified by the large offset of testing temperatures to the glass transition temperature T_g which is close to -70°C for this material [36]. The negligible influence of the test temperature on the mechanical response is checked on the evolution of the stiffness during the fatigue test, for several temperatures (23, 50, 80°C). The relative evolution remains within the scatter for one given temperature. Therefore, the FEA results do not change for different test temperatures. Pure shear, uniaxial compression and confined compression tests are carried out to determine the model parameters. The parameter identification process is based on a fit of the identification-specimens FE-models to the measured displacement-force curves. To exclude the influence of the Mullins effect, some pre-conditioning load-cycles are conducted before the quasi-static parameter identification cycle. The identified model parameters are given in table 5. The volumetric response parameter D_1 might seem so small it could be set to zero, but this slight compressibility is accounted mainly for numerical convenience, a common practice for quasi-incompressible materials [35].

Table 5: Mooney-Rivlin parameters

Parameter	Value
C_{10}	0.367 MPa
C_{01}	0.0444 MPa
D_1	0.000631 MPa^{-1}

3.1.2. Axisymmetric model and FEA mesh

The specimen geometry and all the enforced tension and rotation loads are obviously axisymmetric. The FE-analyses are hence using axisymmetric elements, with a degree of freedom in the axial and radial directions combined with an additional degree of freedom for an axial twist. 4-nodes hybrid elements with bilinear displacement and a constant pressure are used (Abaqus denotation: CGAX4H). The FE mesh is shown in *Figure 14*. The given elements with a side length of approximatively 0.5mm. The choice to analyze mechanical values at the centroid is justified by the requirement to obtain a mean value over the volume of elements. The element is therefore considered as a representative elementary volume, which is for instance justified by the fact that the main target of this study is to compare the calculated and measured crack orientations, the latter that may exhibit a minimum length of 0.5mm to be considered. Observations also confirm that the considered crack depths are similar. The central element is located in the notched area. It reflects for all tension and torsion loads the highest strained element. All following mechanical studies only consider this element, since crack initiation is observed in this specific area.

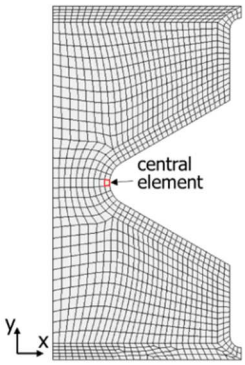

Figure 14: Axisymmetric mesh of the AE2-specimen. In red, the element in the notch ground. All following mechanical studies are evaluated on the centroid of this element.

3.2. Critical plane orientation

The objective of FE calculation is here to predict crack orientations as it is performed in other published studies. Two different critical plane studies were specifically mentioned in section 1 [6,14]. Critical plane methods for elastomeric materials were indeed developed quite simultaneously by Mars and by Saintier. The major assumption is that fatigue cracks propagate on a particular material plane, driven by some mechanical state values. If the global philosophy is identical, the respective approaches are however different in terms of application. As stated by Mars [37], major differences include how the critical plane is selected, what criterion is used to quantify the severity of loading experience on the critical plane, and how damage on the critical plane evolves under solicitation. Here, the main objective is to consider the critical plane approach essentially to give a first

approximation of a crack propagation direction. [6,14] mention the highest maximal principal strain or stress to be orthogonal to the critical material plane (the one in which the crack initiation respectively propagation is expected). Thus, the Saintier's approach is here preferred, and the choice is made to based it on strains instead of stresses for the sake of implementation and as directions are equivalent as stated before. The orientation of these material planes, which are reported as critical, can be determined with the stretch tensors. Their maximal principal orientation is the same as for the maximal principal strains or stresses and they can be computed by the polar decomposition of the deformation gradient tensor $\boldsymbol{F}$:

$$\boldsymbol{F} = \boldsymbol{R}\boldsymbol{U} = \boldsymbol{v}\boldsymbol{R} \tag{9}$$

where $\boldsymbol{R}$ is the rotation tensor, $\boldsymbol{U}$ is the right stretch tensor and $\boldsymbol{v}$ is the left stretch tensor. The two stretch tensors have the same eigenvalues or principal stretches λ_i, but their principal directions differ. The principal directions $\boldsymbol{N}_i$ of $\boldsymbol{U}$ are expressed in the non-deformed material configuration while the principal directions $\boldsymbol{n}_i$ of $\boldsymbol{v}$ are expressed in the deformed material configuration, respectively. The critical plane orientation in every material point is defined here by the highest maximal stretch orientation over time:

$$\lambda_{1,max} = \max_t\big(\lambda_1(t)\big) \Rightarrow \begin{cases} \boldsymbol{n}_{cp} = \boldsymbol{n}_{1,max}(t_c) \\ \boldsymbol{N}_{cp} = \boldsymbol{N}_{1,max}(t_c) \end{cases} \tag{10}$$

where $\lambda_{1,max}$ is the highest maximal stretch over time, $\boldsymbol{n}_{CP}$ and $\boldsymbol{N}_{CP}$ are the normal vectors of the critical plane in the deformed, respectively undeformed configuration, $\boldsymbol{n}_{1,max}$ and $\boldsymbol{N}_{1,max}$ are the principal stretch directions of the highest maximal stretch over time $\lambda_{1,max}$. t_c is the time when $\lambda_1$reaches $\lambda_{1,max}$.

Abaqus simulations provide all mechanical fields in the deformed configuration. However, crack analyses at the surface of the specimen are achieved only on the undeformed configuration. Hence, the critical plane orientations must be transported into the undeformed material configuration. The Nanson's relation between areas in deformed and undeformed states is thus used:

$$da\,\boldsymbol{n} = J\,dA\,\boldsymbol{F}^{-T}\boldsymbol{N} \tag{11}$$

Where $J = \det \boldsymbol{F}$, da is an area in deformed configuration, dA is the same area in the non-deformed configuration, while $\boldsymbol{n}$ and $\boldsymbol{N}$ are their respective outward normal vectors. Even though the FEA model accounts for a slight compressibility, the volume change is negligible for all the tests in this article. Hence, one can assume $J = 1$, which is a common assumption for NR [38]. After all, one can derive for the transformation of the material plane orientation:

$$\boldsymbol{N}(t^*) = \boldsymbol{F}(t^*)^T \cdot \boldsymbol{n}(t^*)\ \frac{1}{\|\boldsymbol{F}(t^*)^T \cdot \boldsymbol{n}(t^*)\|_2} \tag{12}$$

where $\|\cdot\|_2$ denotes the Euclidean norm and $\boldsymbol{N}, \boldsymbol{F}, \boldsymbol{n}$ are related to the same load time t^*. The normalization is here necessary to assure the unity of $\boldsymbol{N}$. As this relationship is valid at any moment of the load, for the critical plane orientation, it comes:

$$\boldsymbol{N}(t_c) = \boldsymbol{F}(t_c)^T \cdot \boldsymbol{n}(t_c) \frac{1}{\|\boldsymbol{F}(t_c)^T \cdot \boldsymbol{n}(t_c)\|_2} \quad (13)$$

To compare the orientation of the plane perpendicular to this maximal principal stretch and of observed crack planes, both are expressed as angles in relation to the radial plane, defined in *Figure 11*. To calculate this angle of the critical plane, the operation is:

$$\alpha_{cp} = \arctan\left(\frac{N_z(t_c)}{N_y(t_c)}\right) \quad (14)$$

where N_y and N_z are the y and z component of the vector $\boldsymbol{N}$.This computed critical plane orientation for different loading conditions will be compared to the experimental crack orientation in the following sections.

4) Results & Analyses

This section presents the test results. We will first present results of test conditions that are already known in the literature: uniaxial tension and torsion tests for relaxing conditions and non-relaxing tension tests. The goal is to crosscheck previous results and then to generate a database on our samples for a comparison with experiences with more complex loading conditions. Secondly, this section will describe the results for multiaxial proportional tests using relaxing loading. Finally, multiaxial test results with sequenced loading using non-relaxing conditions will be detailed.

For each test campaign, we will systematically investigate three main indicators. The first one is related to the lifetime curve evolution, or when available and because it provides a clearer insight, the evolution of the reinforcement factor with reference to a given testing condition. The second one is related to the features of crack population (amount, roughness, branching), as mentioned on *Figure 7*. The third one is finally the comparison between the measured crack orientation and the one predicted using the critical plane approach (see subsection 0). The wide experimental database generated will allow us to discuss the evolution of these three indicators for different loading types (uniaxial, multiaxial, tension, torsion), several load ratios R (inducing relaxing and non-relaxing conditions) and, when available, various temperatures.

4.1. Uniaxial tension and torsion tests for relaxing conditions

The tests given in this sub-section are all conducted with pure tension or pure torsion loads and detailed in Table 1 (tension tests) and Table 2 (torsion tests, reference A). *Figure 15* presents the results of the uniaxial tension fatigue tests as Wöhler curves for 23°C, 50°C, and 80°C.

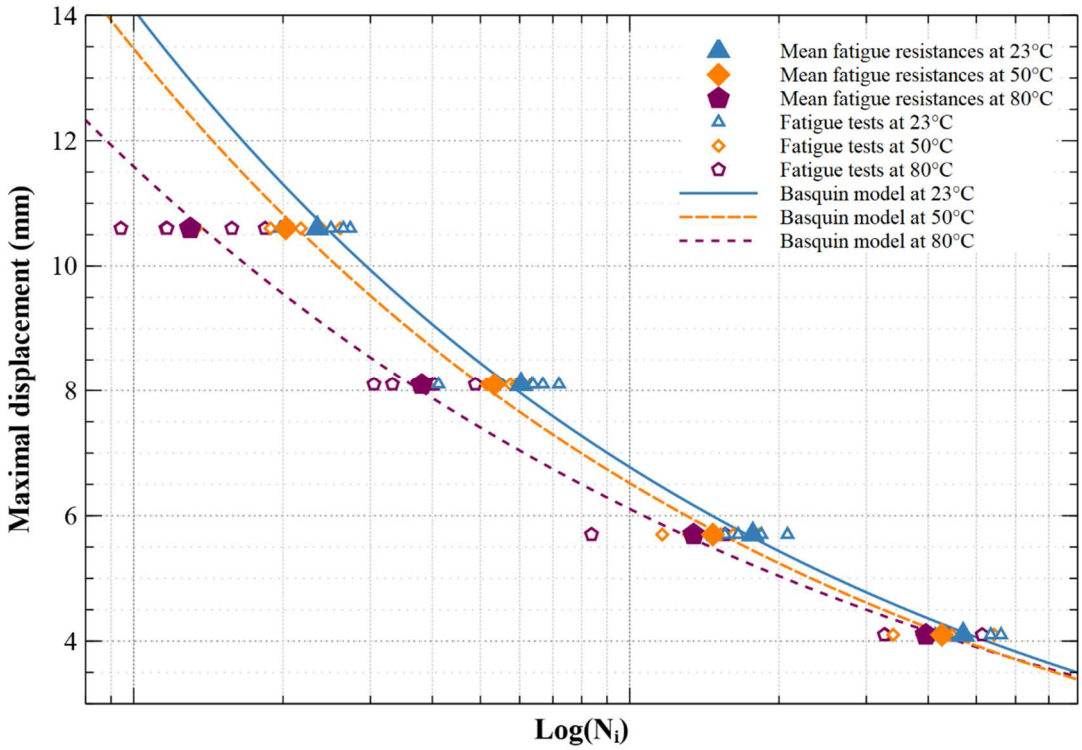

Figure 15: Number of cycles to crack initiation for simple relaxing tension tests with different temperatures.

The Wöhler curves come from relaxing test results, which should experience therefore no material reinforcement. These tests are hence used as reference lifetime conditions for further non-relaxing conditions. For all these conditions, the cracks present very low roughness and almost no branching, as illustrated on the top image of Figure 16. Additionally, the crack orientation is always perpendicular to the tension direction (i.e., 0° angle). The orientation is therefore consistent with the predicted critical plane.

Figure 18 (please see section 4.3) presents the results of the uniaxial torsion fatigue tests. For the sake of limiting the number of Figures, the results are plotted in the same graph as non-relaxing conditions. The results of interest here are the one obtained for pure torsion loading (*i.e.*, null tension displacement), for a given amplitude of 150°. Pure rotation loads are conducted only at room temperature. Their measured lifetimes for $R_\theta = 0$ and $R_\theta = -1$ are taken as a reference for the following. One can observe that lifetimes obtained for $R_\theta = -1$ are approximately half on the ones obtained for $R_\theta = 0$ which might be logical as the $R_\theta = -1$ conditions could be described as two

combined $R_\theta = 0$ cycles in opposite rotation directions. For these two conditions, the cracks present very low roughness and almost no branching, as illustrated on the top images of *Figure 16*.

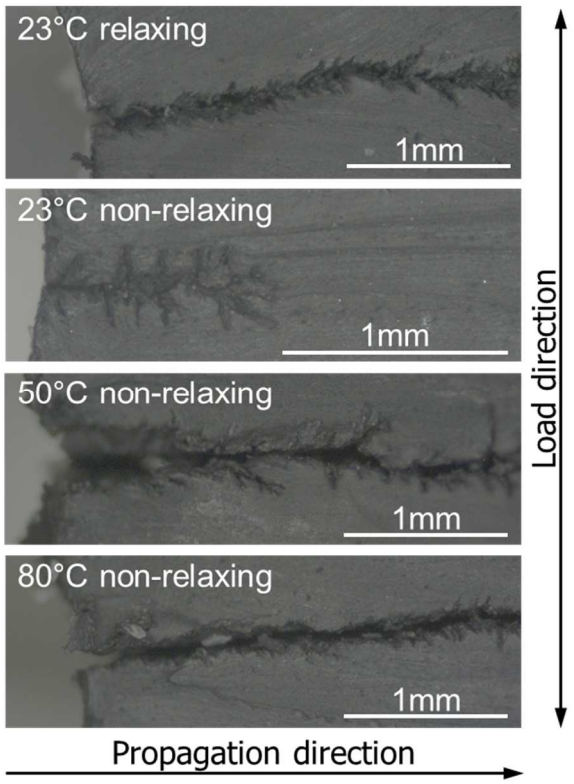

Figure 16: Crack propagation paths for relaxing and non-relaxing load conditions. All shown cracks come from AE2 samples which were loaded in pure tension. The maximum displacement level is 10.6mm for all cracks. Non-relaxing cracks come from minimum displacement levels of 2.65mm.

Figure 20 (please see section 4.3) also provides the crack orientation. For $R_\theta = -1$, two symmetrical crack orientations can be found with an angle of approximately $\pm 12°$. For $R_\theta = 0$, only one crack orientation is observed with a mean angle of approximately $-28°$. The calculated critical plane is estimated at -15°. The FEA predictions also well predict the two opposite critical planes for $R_\theta = -1$, which are different from experiments. Considering the scatter of the experimental data (evaluation over 11 to 21 cracks, see Table 2), the experimental orientations seem reasonably consistent with the critical plane predicted.

As specified previously, fatigue tests are also performed under different temperatures to possibly inhibit the reinforcement effect. It is therefore of paramount importance to evaluate the effect of temperature on fatigue results for relaxing conditions, to highlight the effects specifically related to reinforcement phenomena.

One can observe on *Figure 15* presenting the Wöhler curves that the different testing temperatures do not significantly change the curves' slope, but that a higher temperature significantly decreases specimen lifetime. The mean lifetime at 50°C is only 0.88 times of the one measured at 23°C. This ratio gets down to 0.63 when the test temperature reaches 80°C. This is approximately true for all tension levels due to the similar Basquin slopes.

These findings correspond to what is reported in the literature on NR for relaxing tension tests under different temperatures (see for instance [26]). For all temperatures, the cracks features (limited roughness and branching, 0° orientation) are similar to the results obtained at 23°C. As reported in Table 1, the observed crack orientations are therefore consistent with the predicted crack orientations for pure-tension loads.

4.2. Uniaxial non-relaxing tension tests

The tests given in this sub-section are conducted with pure tension loads with non-relaxing conditions, under various temperatures (23, 50, 80°C) and detailed in Table 1. *Figure 17* highlights the results obtained using an increasing R_{displ} ratio, for a given maximum displacement level (10.6mm).

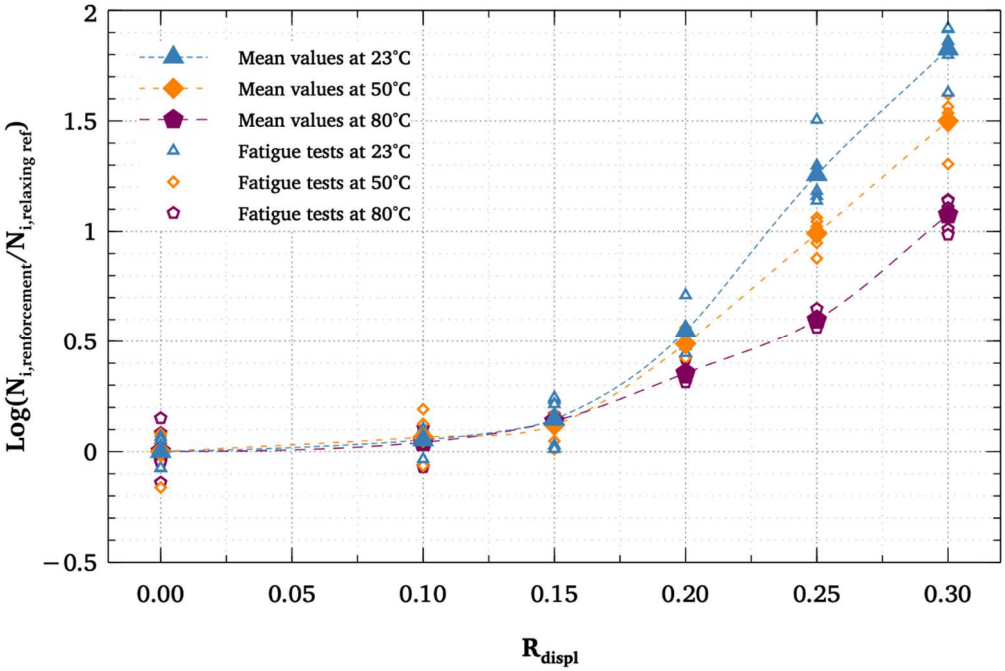

Figure 17: Relative lifetime results of simple reinforcement tests. For each temperature, the reference $Ni_{relaxing}$, is the mean lifetime of the relaxing Wöhler tests at the max. displacement 10.6mm.

The minimal displacement is therefore evolving, as presented in Table 1. It is chosen here to plot the evolution of the material lifetime reinforcement in logarithmic scale to provide a better illustration of the effect of the R_{displ} ratio. It is remarkable to observe that a maximal increase in the fatigue lifetime by a factor of 66 is obtained for a load ratio R_{displ} of 0.3. This result is in line with the observations of Busse [8], lifetime increases as high as a factor of 100. *Figure 17* also presents the evolution of the reinforcement factors for test temperatures of 50°C and 80°C. One can observe a major drop of the reinforcement effect with temperature. For the highest ratio $R_{displ} = 0.3$, the factor drops from 66 at 23°C to 32 at 50°C and to only 12 at 80°C. The relative drop is therefore 50% at 50°C and 80% at 80°C. These figures are to be compared to the relative drops obtained for relaxing conditions under temperature: 12% at 50°C and 37% at 80°C. One can therefore conclude that the temperature effect on

reinforcement is clear and significant. This remarkable effect on the fatigue properties is not found very often in the literature (see for instance [26]), whereas several publications report a decrease of crystallization in natural rubber materials with higher temperatures. It therefore seems that the evolution of the reinforcement effect may be related to the crystallization that occurs under cyclic loading. This point is discussed in Section 4.5.

Dealing with the features of the cracks, a comparative study of the crack propagation paths is given in *Figure 16*. If we first compare the cracks obtained at 23°C for relaxing and non-relaxing conditions, the latter clearly exhibits more crack branching than the first ones. Under non-relaxing conditions, the degree of this displayed branching phenomenon is decreasing as the testing temperature increases, and is almost invisible at 80°C. These findings are in line with the work of Saintier *et al*. [10] (see section 1.2). They report that this phenomenon is connected to strain-induced crystallization. As a conclusion here, crack branching is supposed to be strongly related to fatigue reinforcement while temperature is reducing both phenomena progressively. As mentioned in Table 1, the crack orientations are found, in every case, perpendicular to the tension direction for uniaxial tension tests, whatever the temperature or load ratio. The experimental data are therefore consistent with the orientation predicted by the critical plane FE computations.

4.3. Multiaxial proportional tests under relaxing conditions

The results obtained using coupled and proportional rotation and displacement actuators are now being investigated and the details are given in Table 2, reference E. The proportional coupling of both actuators is set to ensure relaxing test conditions by returning to 0 for torsion and tension axis. These tests have been performed with three objectives. The first one is to act as reference tests for the following non-relaxing and sequenced multiaxial tests. The second objective is to investigate the ability of the critical plane approach to predict the crack orientation under these complex loading conditions. The third objective is finally to evaluate the influence of temperature on the fatigue lifetimes for multiaxial non-relaxing conditions.

The fatigue lifetimes for tests performed at 23°C are given in *Figure 18*. The comparison of the results obtained for the two proportional loads, (with a maximal rotation angle of $\theta = 150°$) with the ones obtained under simple torsion tests for $R_{displ} = 0$ and of $\theta = 150°$ show no increase in lifetime. This observation proves that the chosen multiaxial conditions can be considered relaxing ones.

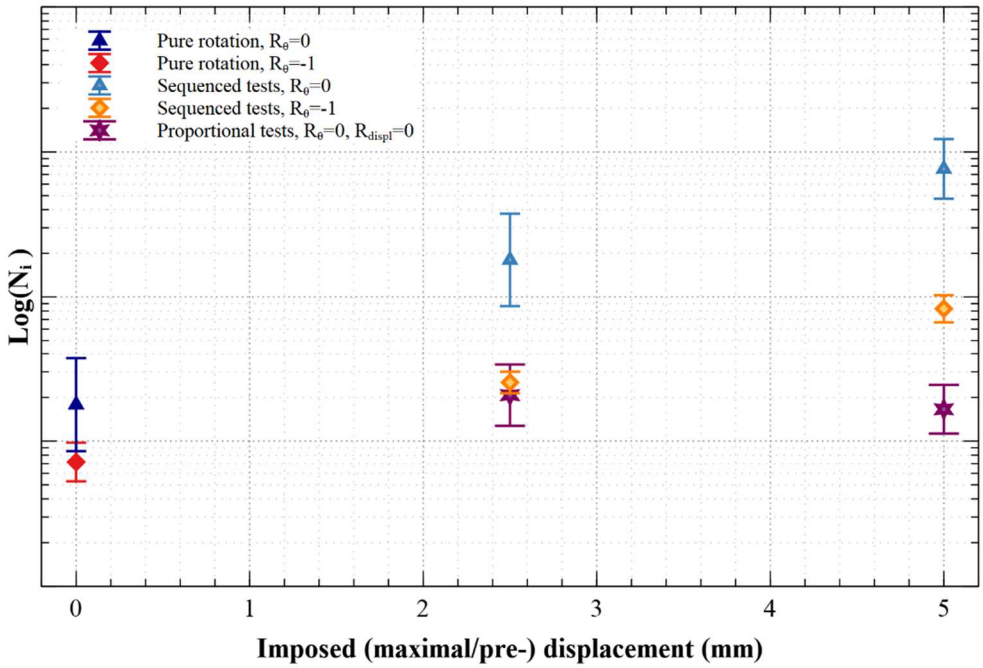

Figure 18: Average number of cycles until crack initiation for different test conditions at room temperature. The error bars reflect $\pm 2 \cdot$ standard deviation.

Figure 19 illustrates the cracks obtained for these conditions (right hand column): they present very low roughness and no branching.

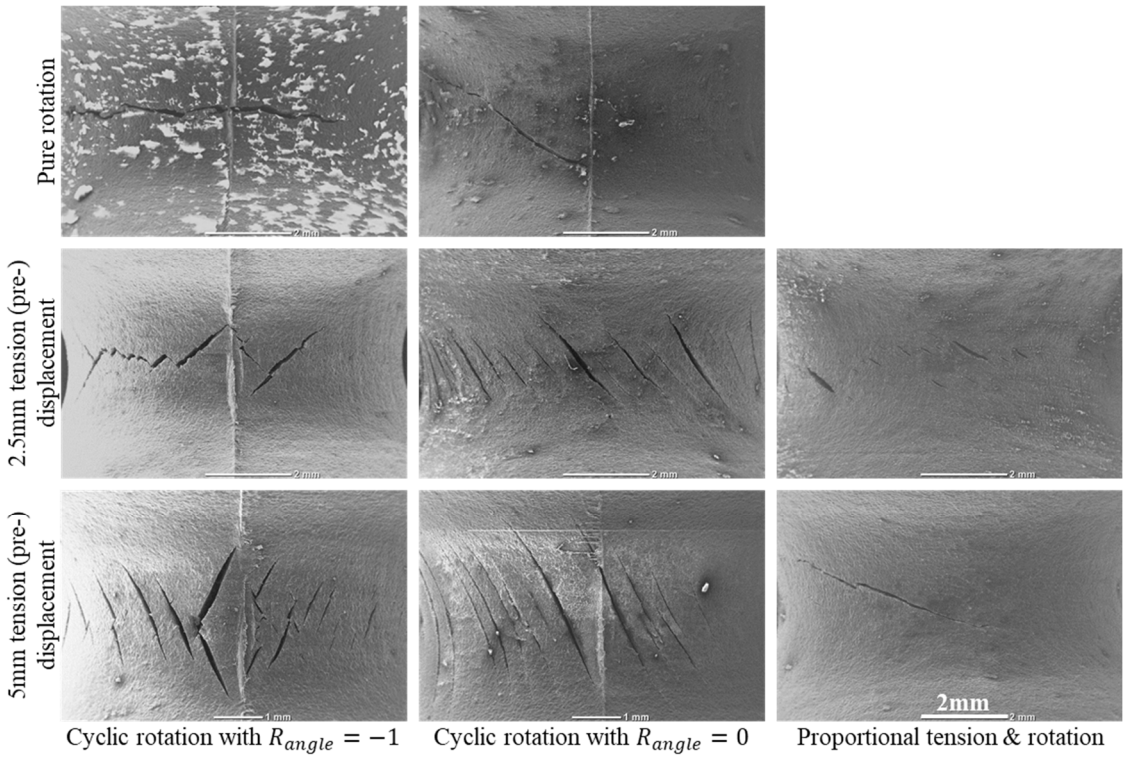

Figure 19: Exemplary SEM specimen surface studies of different load levels.

The crack orientations observed and predicted for these proportional tests are plotted in *Figure 20* and compared with sequenced multiaxial tests. First focusing on the results of proportional tests (star markers and dotted line for $\theta_{max} = 150°$), the measured and predicted values appear to be not aligned. However, the observed difference remains limited and is almost within the experimental scatter (40 cracks measured, see Table 2). This therefore confirms that cracks observed for tests with no material reinforcement (as given in *Figure 7*) and for tests for proportional multiaxial loadings exhibit the same kind of feature.

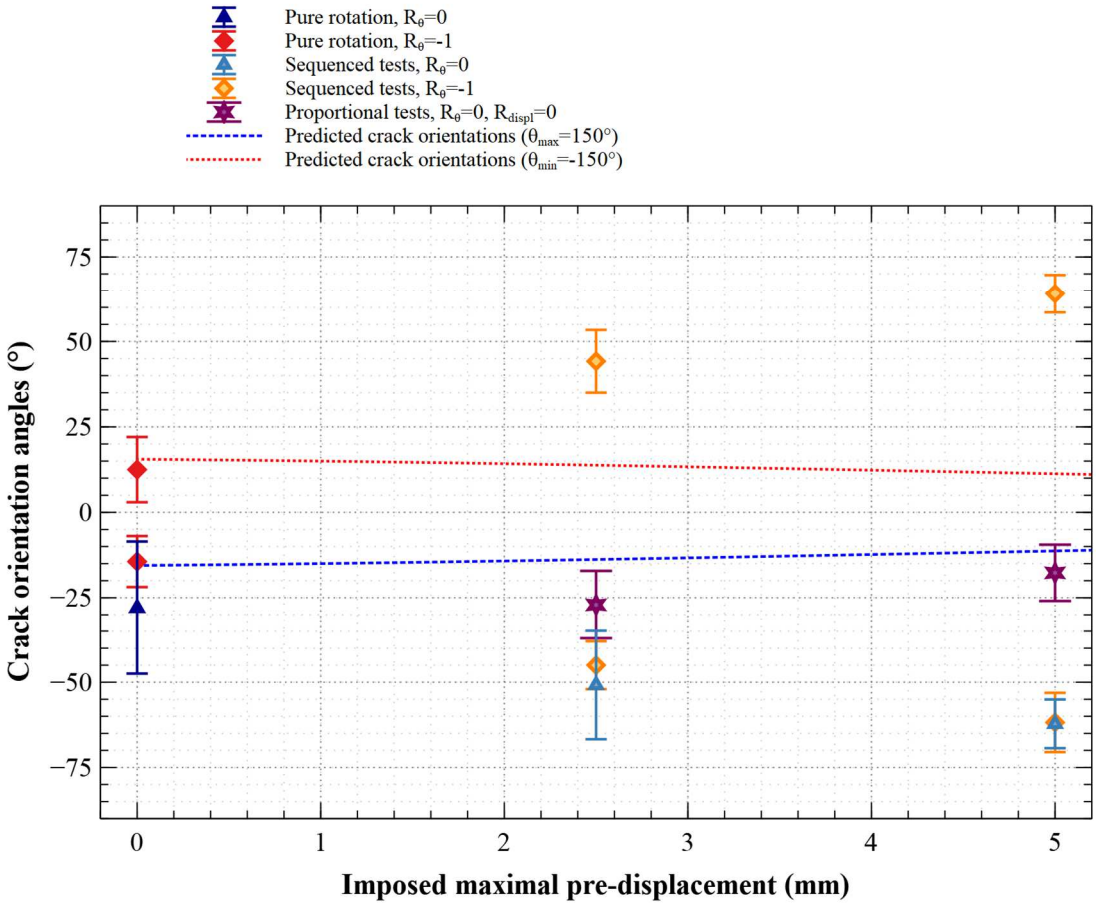

Figure 20: Measured average crack orientation angles for different test conditions at room temperature. The error bars reflect $\pm 2 \cdot$ standard deviation.

An additional test is conducted at 80°C (see *Figure 21* (section 4.4) for the lifetime and *Figure 23* (section 4.4) for the measured crack orientations). The high temperature causes here a 72% lifetime decrease in comparison to the same proportional test at 23°C. This is a higher decrease than the one measured for pure tension loads with the above given Wöhler curves at 23°C and 80°C. Here again, the orientations of the measured and predicted cracks are aligned.

4.4. Multiaxial sequenced loads for non-relaxing conditions

This section presents the results obtained with pre-displacements in tension and cyclic rotations (see table 2, reference C and D). These kinds of tests and their analyses of crack features are new to the literature, to the knowledge of the authors.

The pre-displacement is set to either 2.5mm or 5mm, with following rotation cycles in sequence. This constant displacement level keeps the specimen in a permanent non-relaxed state. The sequenced test conditions are therefore meant to be non-relaxing (*i.e.*, conditions leading to fatigue reinforcement) loads. The objective is to challenge the usual results obtained for uniaxial non-relaxing tests for multiaxial testing conditions. The database of sequenced test results is therefore extensive. It includes tests with two different levels of pre-displacements, combined with 4 different rotation ratios R_θ and 4 different test temperatures.

The influence of the load ratio ($R_\theta = 0$ & -1) on the reinforcement and on the crack orientations obtained for multiaxial sequenced tests is first highlighted in this section. Moreover, for $R_\theta = 0$, the sequenced tests (constant tension and cyclic torsion) are compared with the relaxing proportional tests (tension and torsion) for the same maximum angle of 150°. The temperature is 23°C for all testing conditions.

Figure 18 provides a comparison of the lifetimes for these tests. Considering the evolution of the reinforcement for sequenced tests performed using an angle ratio $R_\theta = 0$ (triangle markers), one can see that the lifetime is increasing when the imposed tension displacement increases, despite a minimal angle in torsion kept equal to zero. The reinforcement factor is about 8.7 at 2.5mm and 46 at 5mm for this load ratio. These high reinforcement factors are of the same order of magnitude as the ones obtained for uniaxial tension tests with minimum displacement values between 2 and 3.2 mm (see Table 1, Reinf_23degC series). Comparing now the results obtained for sequenced and proportional tension-torsion tests for the same load ratio of $R_\theta = 0$ (comparison between triangle and star markers), it is clearly observable that the reinforcement effect is not seen for proportional tests and is therefore directly related to the imposed pre-tension.

Focusing now on the results obtained for $R_\theta = -1$ (diamond markers), the reinforcement effect is again clearly visible and increasing with the pre-tension level. The reinforcement factor is about 3.5 at 2.5mm and 11.6 at 5mm for this R_θ-ratio. The relative evolution therefore exhibits the same trend for both load ratios ($R_\theta = 0$ & -1), but the reinforcement effect is higher for a torsion angle ratio $R_\theta = 0$.

Figure 19 compares evolution of the crack population for the same tests with two main noticeable observations. Firstly, for $R_\theta = -1$, two symmetrical cracks populations are visible, which was already notified for relaxing conditions in section 4.1, but appears in an even clearer way for non-relaxing testing conditions here. Only one

crack orientation is on the contrary observed for $R_\theta = 0$. For all sequential loadings, the measured crack orientations show a clear principal direction. The second observation is related to the crack angles as they depend on the loading history and evolve sensibly with the tension pre-displacement. *Figure 20* provides a quantitative evaluation of the crack angles and a comparison to the crack orientation that may be predicted following a critical plane approach. It appears clear that for both load ratios, as soon as the loading conditions involve a reinforcement, the crack orientations predicted from the critical plane approach are not matching the experimental observations, whatever the load ratio or the applied pre-displacement in tension. A larger deviation is furthermore observed for the highest reinforcement factors. The crack directions deviate by more than 30° from the predicted crack plane at 2.5mm pre-displacement and by more than 50° at 5mm pre-displacement. Another key observation is that the crack orientation is completely consistent for both load ratio and seems therefore connected only to the maximum angle imposed (150°, here). Interestingly, the relative reinforcement factor is not the same for both load ratios. This would mean that the increase in lifetimes is not only related to the crack deviation/angle and that the phenomena at stake at the crack tip are acting not only on the crack propagation angle, but also on the crack growth rate. To our knowledge, these observations have not been reported in the literature yet.

In the following, we now focus on the influence of temperature on multiaxial sequenced tests for a tension pre-displacement of 5mm, with cyclic rotations of ratios $R_\theta = 0$ & -1, and for temperatures of 23, 50, 60, 70, and finally 80°C.

Figure 21 plots the measured lifetimes as a function of the test temperature. As previously, the reference-relaxing results are given by the proportional multiaxial test (star markers at 20 and 80°C). The first observation is that the reinforcement effect is decreasing significantly with increasing test temperatures, for both load ratios. The reinforcement factors drop for instance from 46 at 23°C to 16.4 at 80°C for $R_\theta = 0$. The relative drop in lifetimes is also of high interest. When considering the reference relaxing proportional tests, the previously observed relative drop of lifetime between tests at 23°C and at 80°C is of 72%. For the multiaxial sequenced tests, this relative drop is of 90% for $R_\theta = 0$ and 87% for $R_\theta = -1$. It can be concluded that the test temperature has an effect on both relaxing and non-relaxing tests but that this effect is even stronger on non-relaxing test. If we now take a closer look to the relative curve evolutions, they appear to be very comparable for both load ratios. We observe a rather progressive decrease with temperature up to 70°C (similar indeed to the decreasing trend observed for relaxing tests) and a more sudden drop after 70°C. This progressive drop seems consistent with previous observations from pure tension tests of Le Chenadec [39]. To our knowledge, these observations of the influence of temperature on multiaxial fatigue are original.

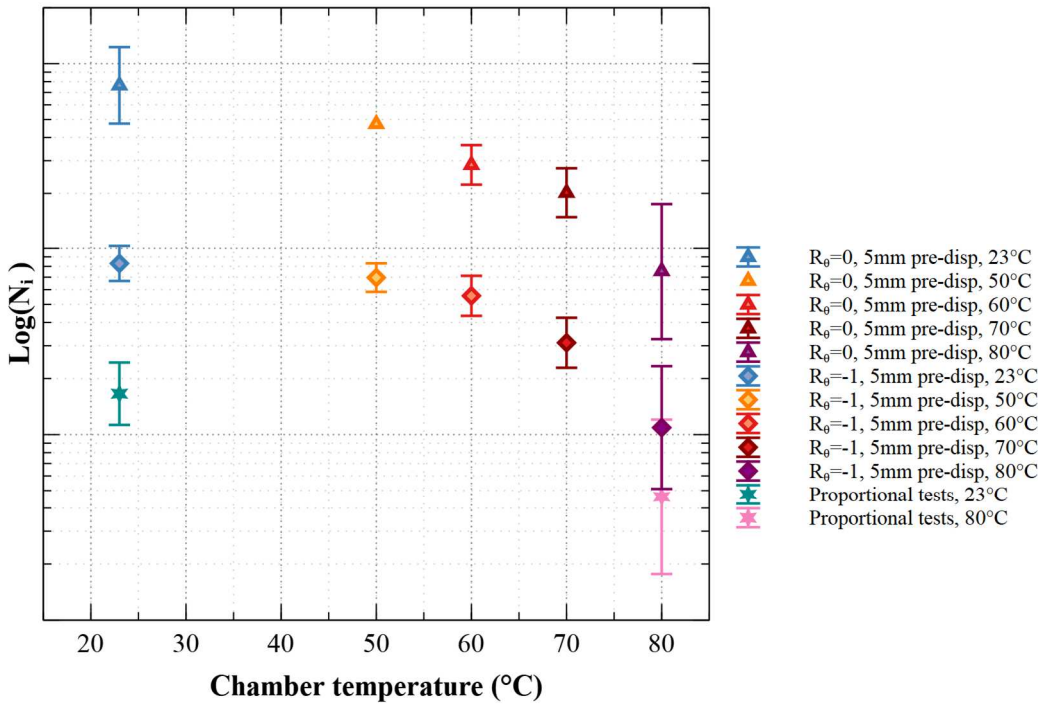

Figure 21: Average number of cycles until crack initiation for different test conditions. The error bars reflect $\pm 2 \cdot$ standard deviation.

Figure 22 exhibits the crack population for the tests performed at 23 and 80°C for the reference test (column 5), $R_\theta = -1$ (column 1) and $R_\theta = 0$ (column 4). For non-relaxing tests, the crack orientations at 80°C and 23°C are here very different for both load ratios, while the orientation at 80°C tends to align with the one observed for relaxing tests.

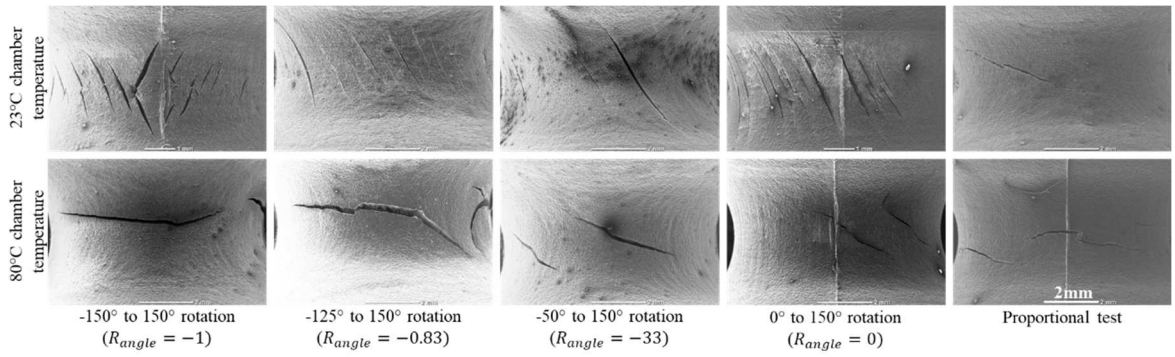

Figure 22: Exemplary SEM specimen surface studies of different load levels and different test temperatures (pre-displacement is always 5mm here).

Figure 23 provides a full and quantitative view if the evolution of the crack orientation with the test temperature and compares the measured crack orientations to the predictions obtained following a critical plane approach. The measured population of angles here shows a higher scattering with higher temperatures, similar in amplitude to the one observed for lifetime in comparable loading conditions. The second noticeable observation is that two

crack populations with symmetrical orientation appear for tests at $R_\theta = -1$, whatever the test temperature. On the second hand, the angles obtained for tests at $R_\theta = 0$ and $R_\theta = -1$ are consistent whatever the test temperature. The last and most important observation is of course the progressive alignment of the crack orientations with the predicted ones (relying on critical plane approach) as the test temperature increases. For the tests performed at 80°C, the observed cracks are perfectly aligned with the orientation predicted from the critical plane approach and with the relaxing tests, while, in spite of a large scattering, the deviation seems visible at 70°C and drastically increases for lower temperatures.

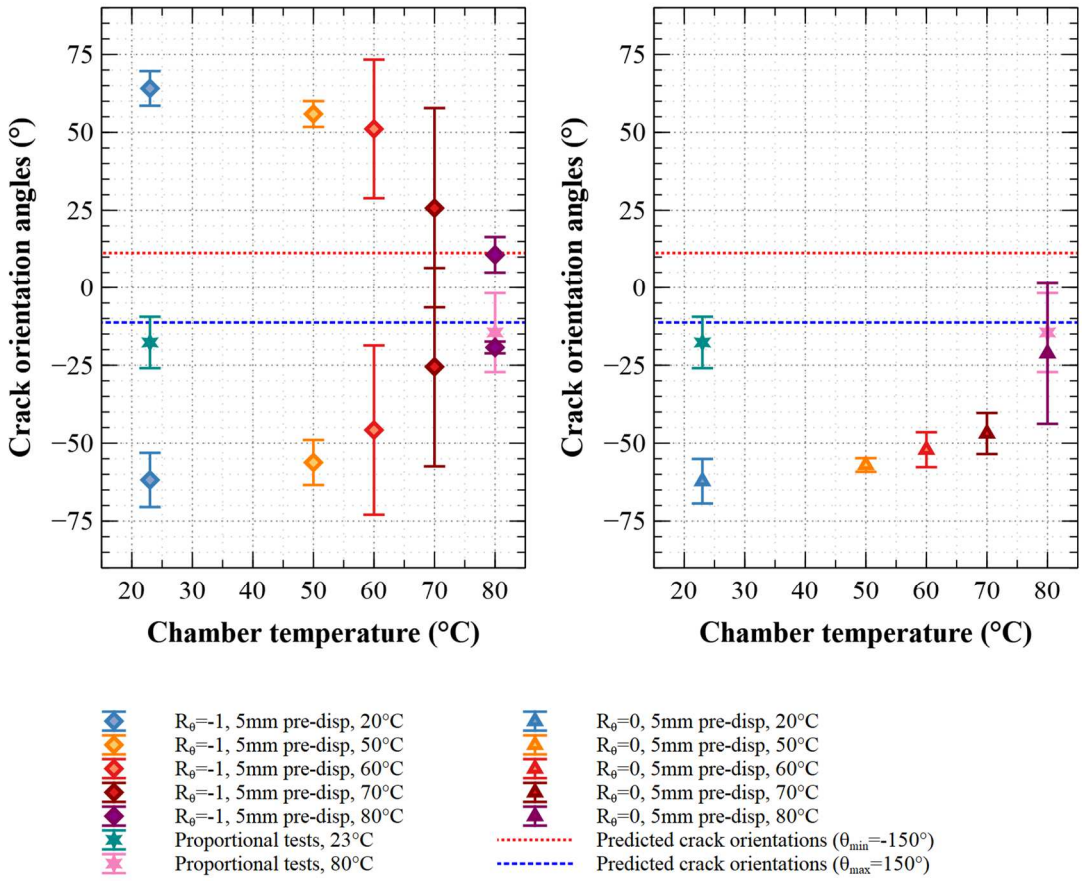

Figure 23: Measured average crack orientation angles for different test conditions. The error bars reflect $\pm 2 \cdot$ standard deviation.

It is interesting to underline here that these evolutions of the crack orientation deviation seem very similar to ones observed for the lifetime reinforcement. These observations of lifetime reinforcements and crack features for high temperatures are also unprecedented in the literature for natural rubber materials and underline the strong effect of multiaxial loading and environment effects for this material.

The previous paragraphs investigated the influence of the pre-displacement for two different load ratios R_{displ} (0 and -1) and the influence of temperature. A last campaign has been achieved to enlarge the investigation on the

load ratio in rotation (R_θ) on the crack orientation. Keeping a maximal rotation angle of 150° and a pre-displacement of 5mm, tests have been performed for different rotation ratios of $R_\theta = 0, -0.33, -0.83$ & -1. These tests have been performed at 23°C and 80°C to once again investigate the temperature effect.

Figure 24 gives the measured crack orientation populations for both temperatures as a function of the minimum rotation angle. The measurements are compared to the orientation predicted by the numerical simulations using the critical plane approach. The results underline that even when the load ratio in torsion R_θ is close to -1, only a single orientation is observed. The two crack populations are observed only for $R_\theta = -1$. This result is also visible in *Figure 22*, presenting the crack observations. The results also show that the measured crack angle populations are almost constant for the different ratios R_θ. The measured principal crack orientation depends therefore only on the highest rotation angle during the cyclic loads. This conclusion is confirmed for the two tested temperatures. At 80°C, the crack orientation is indeed similar to relaxing tests (*i.e.,* star markers for proportional multiaxial tests), whatever the minimum angle imposed. At 23°C, the angles measured are clearly different and similar to the tests exhibiting strong reinforcement (diamond markers, $R_\theta = -1$, or triangle markers, $R_\theta = 0$). The variation of the torsion load ratio between 0 and -1 does not affect the obtained angles, for both temperatures. When it comes to the comparison with numerical predictions, first, the appearance of two crack angle populations only for $R_\theta = -1$ is well predicted by FEA. Second, for tests performed at 80°C, the agreement between experiments and simulations is fairly good, which is consistent with a low, if any, reinforcement, as seen previously for $R_\theta = -1$ and $R_\theta = 0$. Third, for tests performed at 23°C, the crack angles deviate from the critical plane prediction, which is also consistent with previous tests at $R_\theta = -1$ and $R_\theta = 0$.

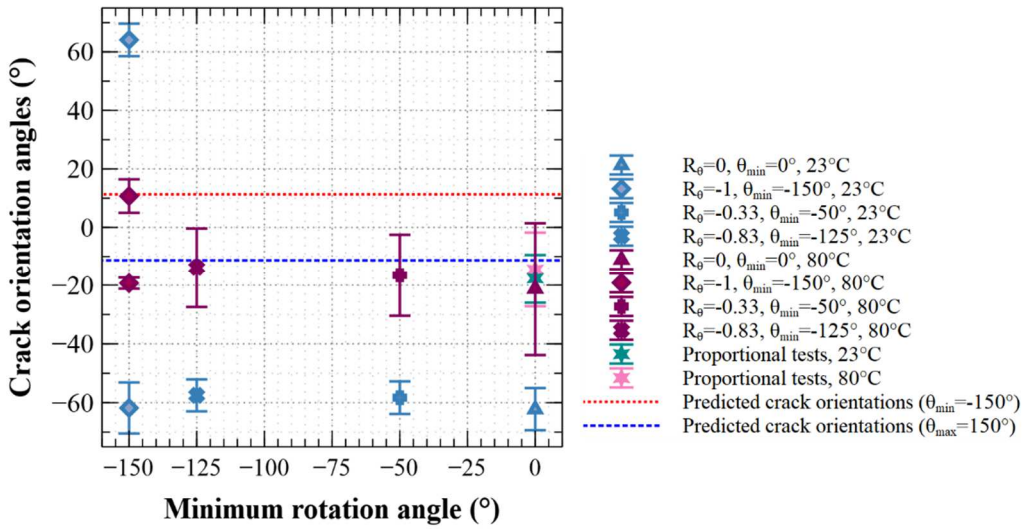

Figure 24: Measured average crack orientation angles for different test conditions. The error bars reflect $\pm 2 \cdot$ standard deviation.

4.5. Synthesis

The main objective of this study was to provide a quantitative database on lifetime reinforcement under tension-torsion loading, both for relaxing and non-relaxing conditions. The listed results and its presentation with different factors on study already give a deep insight into the lifetime reinforcement and the crack features of natural rubber under uniaxial and multiaxial loadings. The principal observations are the following:

- For uniaxial loading under relaxing conditions, results from the literature have been confirmed under pure tension or pure torsion tests at 23°C. The crack presents a low roughness, no branching, and their orientations are consistent with the ones predicted from a critical plane approach. For tension tests performed at 50 and 80°C, a respective mean lifetime reduction of 12% and 37 % is observed, despite no signs of thermal ageing;
- For uniaxial tension test under non-relaxing conditions at 23°C, a strong reinforcement can be observed (up to a ratio of 66), with cracks presenting a high roughness, visible branching. The direction of crack propagation is more disturbed but correlates well with a prediction based on a critical plane approach. For tension tests performed at 50°C and 80°C, and a load ratio $R_{displ} = 0.3$, a respective lifetime reduction of 50 % and 80 % is observed. The comparison with the previous results obtained for relaxing tests illustrates that temperature has a specific inhibition effect on fatigue reinforcement. The features of the cracks also support this conclusion as they are less and less rough and branched as the test temperature increases;
- For multiaxial proportional tests under relaxing conditions at 23°C, it can be observed that whatever the tension-torsion combination, the crack orientations are consistent with the ones predicted using a critical plane approach. Tests performed at 80°C shows that the high temperature causes a lifetime decrease of 72 % in comparison to the same proportional test at 23°C. This decrease is higher compared to the one measured for relaxing pure tension loads. This result was not expected and could be explained by less oriented elastomeric network under combined multiaxial load;
- For multiaxial sequenced tests under non-relaxing conditions (*i.e.*, torsion cyclic tests with a tension preload) at 23°C, many parameters have been tested leading to many conclusions. A clear reinforcement effect can be observed (up to a factor by 46 for $R_\theta = 0$ and up to 11.6 for $R_\theta = -1$). This reinforcement factor is increasing with the tension preload. The cracks present visible roughness and branching and the crack orientation is repeatable (*i.e.*, similar for all cracks observed for a given test condition). Except for a load ratio $R_\theta = -1$, where 2 cracks populations have been observed presenting symmetric angles, only

one angle has been observed. The difference between the reinforcement for the two load ratios could come from the fact that two crack populations are observed for $R_\theta = -1$. A major result is that the crack orientation is clearly not consistent with the one predicted from a critical plane approach, whatever the test conditions. The deviation can be as large as 50°. For tests performed at higher temperatures (50, 60, 70, 80°C), a progressive drop of the reinforcement effect is visible up to 70°C (similar indeed to the decreasing trend observed for relaxing tests) and a more sudden drop after 70°C. The evolutions are very comparable for both load ratios, with a factor drop of 90% for $R_\theta = 0$ and 87% for $R_\theta = -1$ at 80°C. The cracks observed for these conditions present reduced roughness and branching with increasing temperature. The crack orientations are also progressively aligning towards the orientation predicted by a critical plane approach, as the temperature increases. At 80°C, experimental and predicted orientations are the same. Similar trends are visible on additional tests performed for intermediate torsion load ratios ($R_\theta = -0.83$ and -0.33).

5) Conclusions

This study provides an analysis over an extensive multiaxial and uniaxial fatigue test campaign on CB filled natural rubber (240 samples tested). This database includes relaxing uniaxial tests under tension and torsion for relaxing and non-relaxing tension tests for 3 temperatures and relaxing or non-relaxing multiaxial tension-torsion tests, for up to 5 different temperatures. The main objective of the paper was to challenge the usual observations and critical plane predictions for relaxing and non-relaxing conditions under complex non-relaxing loads. To do so, three indicators have been analyzed: the relative improvement on fatigue lifetime, the cracks features (roughness and branching, from optical and SEM observations) and the comparison to the crack orientation predicted using a critical plane approach. Different conclusions can be drawn through the database analysis. The observations, for uniaxial or multiaxial tests, first confirm the connection between lifetime reinforcement and crack features (roughness, branching). It can also be observed that test temperature has an effect on both relaxing and non-relaxing tests, but that the effect is even stronger on non-relaxing test. Moreover, the predictions of the crack orientation based on the critical plane approach are consistent for both uniaxial and multiaxial tests presenting no or low reinforcement effects (induced by loading or temperature). For conditions leading to reinforcement, the predictions from a critical plane approach based on the principal stretches lead to a reasonable prediction for uniaxial tension conditions. Nevertheless, the predictions are clearly wrong for all tested reinforcing multiaxial configurations. A perspective would be to test the approach either with a constitutive model considering

the possible modification of the material, or with a different criterion to define the critical planes. One can see that the correlation between roughness, branching, reinforcement and the effect of temperature is clearly pointing to a local modification of the microstructure. Nevertheless, the question of the phenomena explaining reinforcement is not solved yet, because the options of local anisotropy, associated or not to crystallization are still open. Further studies are necessary, with more direct access (using WAXD measurements for example) to the microstructural features.

Acknowledgements

The authors would like to thank ANRT for its financial support (grant number 2018/0904).

References

[1] Narynbek Ulu K, Huneau B, Le Gac P-Y, Verron E. Fatigue resistance of natural rubber in seawater with comparison to air. International Journal of Fatigue 2016;88:247–56. https://doi.org/10.1016/j.ijfatigue.2016.03.033.

[2] Le Cam J-B, Huneau B, Verron E. Description of fatigue damage in carbon black filled natural rubber. Fatigue & Fracture of Engineering Materials & Structures 2008;31(12):1031–8. https://doi.org/10.1111/j.1460-2695.2008.01293.x.

[3] Svensson S. Testing methods for fatigue properties of rubber materials and vibration isolators. Polymer Testing 1981;2(3):161–74. https://doi.org/10.1016/0142-9418(81)90002-7.

[4] Cadwell S. Dynamic fatigue life of rubber. Industrial and Engineering Chemistry 1940;12(1):19–23.

[5] Oshima H, Aono Y, Noguchi H, Shibata S. Fatigue Characteristics of Vulcanized Natural Rubber for Automotive Engine Mounting (Characteristics of Composition and Mechanical Properties). Memoirs of the Faculty of Engineering, Kyushu University 2007;67(2):75–83.

[6] Saintier N, Cailletaud G, Piques R. Multiaxial fatigue life prediction for a natural rubber. International Journal of Fatigue 2006;28(5):530–9.

[7] Mars WV, Fatemi A. Experimental Investigation of Multiaxial Fatigue in Rubber. 6th International Conference on Biaxial/Multiaxial Fatigue and Fracture 2003.

[8] Busse WF. Tear Resistance and Structure of Rubber. Rubber Chemistry and Technology 1935;8(1):122–37. https://doi.org/10.5254/1.3548279.

[9] Champy C, Le Saux V, Marco Y, Charrier P, Hervouet W. On the use of a full Haigh diagram for lifetime prediction of rubber parts. In: Marvalová B, Petríková I, editors. Constitutive models for rubber IX. London; 2015, p. 551–557.

[10] Saintier N, Cailletaud G, Piques R. Cyclic loadings and crystallization of natural rubber: An explanation of fatigue crack propagation reinforcement under a positive loading ratio. Materials Science and Engineering: A 2011;528(3):1078–86.

[11] Mars WV, Fatemi A. Fatigue crack nucleation and growth in filled natural rubber. Fatigue Fract Engng Mater Struct 2003;26(9):779–89. https://doi.org/10.1046/j.1460-2695.2003.00678.x.

[12] Lake GJ, Lindley PB. Cut Growth and Fatigue of Rubbers: II. Experiments on a Noncrystallizing Rubber. Journal of Applied Polymer Science 1964;8(2):707–21.

[13] Rublon P. Etude expérimentale multi-échelle de la propagation de fissure de fatigue dans le caoutchouc naturel [PhD Thesis]. Nantes: Ecole Centrale de Nantes (ECN); 2013.

[14] Mars WV. Cracking Energy Density as a Predictor of Fatigue Life under Multiaxial Conditions. Rubber Chemistry and Technology 2002;75(1):1–17. https://doi.org/10.5254/1.3547670.

[15] Ostoja-Kuczynski E. Comportement en fatigue des élastomères: application aux structures antivibratoires pour l'automobile [PhD Thesis]: Ecole Centrale de Nantes (ECN); 2005.

[16] Mars WV, Fatemi A. A Phenomenological Model for the Effect of R Ratio on Fatigue of Strain Crystallizing Rubbers. Rubber Chemistry and Technology 2003;76(5):1241–58. https://doi.org/10.5254/1.3547800.

[17] Lindley PB. Relation between hysteresis and the dynamic crack growth resistance of natural rubber. International Journal of Fracture 1973;9(4):449–62. https://doi.org/10.1007/BF00036325.

[18] Griffith AA. The Phenomena of Rupture and Flow in Solids. Philosophical Transactions of the Royal Society A: Mathematical, Physical and Engineering Sciences 1921;221(582-593):163–98. https://doi.org/10.1098/rsta.1921.0006.

[19] Katz JR. Röntgenspektrographische Untersuchungen am gedehnten Kautschuk und ihre mögliche Bedeutung für das Problem der Dehnungseigenschaften dieser Substanz. Naturwissenschaften 1925;13(19):410–6. https://doi.org/10.1007/BF01560952.

[20] Huneau B. Strain-induced cristallization of natural rubber: a review of X-ray diffraction investigations: R16, 49, 53, 54, 83. Rubber Chemistry and Technology 2011;84(3):425–52.

[21] Lake GJ. Fatigue and Fracture of Elastomers. Rubber Chemistry and Technology 1995;68(3):435–60.

[22] Kawai H. Dynamic X-ray diffraction technique for measuring rheo-optical properties of crystalline polymeric materials. Rheol Acta 1975;14(1):27–47. https://doi.org/10.1007/BF01527209.

[23] Beurrot-Borgarino S. Cristallisation sous contrainte du caoutchouc naturel en fatigue et sous sollicitation multiaxiale [PhD Thesis]: Ecole Centrale de Nantes (ECN); 2013.

[24] Brüning K, Schneider K, Roth SV, Heinrich G. Strain-induced crystallization around a crack tip in natural rubber under dynamic load. Polymer 2013;54(22):6200–5. https://doi.org/10.1016/j.polymer.2013.08.045.

[25] Beurrot-Borgarino S, Huneau B, Verron E, Rublon P. Strain-induced crystallization of carbon black-filled natural rubber during fatigue measured by in situ synchrotron X-ray diffraction. International Journal of Fatigue 2013;47:1–7. https://doi.org/10.1016/j.ijfatigue.2012.07.001.
[26] Charrier P. Influence of temperature on durability behavior of carbon black filled natural rubber. In: Heinrich G, Kaliske M, Lion A, Reese S, editors. Constitutive Models for Rubbber VI. London: Taylor & Francis; 2009, p. 179–185.
[27] Marchal J. Cristallisation des caoutchoucs chargés et non chargés sous contrainte Effet sur les chaînes amorphes [PhD Thesis]: Université Paris XI Orsay; 2006.
[28] Ostoja-Kuczynski E, Charrier P, Verron E, Marckmann G, Gornet L, Chagnon G. Crack initiation in filled natural rubber: experimental database and macroscopic observations. In: Constitutive models for rubber III: Proceedings of the Third European Conference on Constitutive Models for Rubber, 15-17 September 2003, London, UK. Lisse [Netherlands], Exton, PA: A.A. Balkema; 2003, p. 41–47.
[29] Broudin M, Le Saux V, Marco Y, Charrier P, Hervouet W. Investigation of thermal aging effects on the fatigue design of automotive anti-vibration parts. Constitutive Models for Rubber IX 2015:53–9.
[30] Le Gac PY, Le Saux V, Paris M, Marco Y. Ageing mechanism and mechanical degradation behaviour of polychloroprene rubber in a marine environment: Comparison of accelerated ageing and long term exposure. Polymer Degradation and Stability 2012;97(3):288–96.
[31] Basquin O. The exponential law of endurance tests. ASTM Proceeding 1910;10:625–30.
[32] Warneboldt I, Szmytka F, Raoult I, Marco Y, Le Saux V, Charrier P et al. Multiaxial fatigue under complex non-relaxing loads. In: Huneau B, Le Cam J-B, Marco Y, Verron E, editors. Constitutive models for rubber XI: Proceedings of the 11th European conference on constitutive models for rubber, Nantes, France, 25-27 June 2019. Boca Raton: CRC Press; 2019, p. 417–422.
[33] Mooney M. A Theory of Large Elastic Deformation. Journal of Applied Physics 1940;11(9):582–92. https://doi.org/10.1063/1.1712836.
[34] Rivlin RS. Large Elastic Deformations of Isotropic Materials. IV. Further Developments of the General Theory. Philosophical Transactions of the Royal Society A: Mathematical, Physical and Engineering Sciences 1948;241(835):379–97. https://doi.org/10.1098/rsta.1948.0024.
[35] ABAQUS/CAE User's Guide: Abaqus 6.14. Dassault Systèmes; 2014.
[36] Gent AN. Engineering with rubber: How to design rubber components. 3rd ed. Munich, Cincinnati: Hanser Publishers; 2012.
[37] Mars WV. Critical Plane Analysis of Rubber. In: Heinrich G, Kipscholl R, Stoček R, editors. Fatigue Crack Growth in Rubber Materials: Experiments and Modelling. Cham: Springer International Publishing; 2021, p. 85–107.
[38] Holzapfel GA. Nonlinear solid mechanics: A continuum approach for engineering. Chichester: J. Wiley; 2010.
[39] Le Chenadec Y. Autoéchauffement, fatigue thermomécanique des élastomères [Thèse de doctorat]: Ecole Polytechnique X; 2008.